Master Thesis
TVVR 20/5013

Beach Nourishment at Faxe Ladeplads in Zealand, Denmark

- Evaluation and Assessment of Morphological Evolution

Anna Adell

Division of Water Resources Engineering
Department of Building and Environmental Technology
Lund University

Beach Nourishment at Faxe Ladeplads in Zealand, Denmark

Evaluation and Assessment of Morphological Evolution

Author
Anna Adell

Supervisors

Björn Almström and Magnus Larson
Water Resources Engineering

Per Sørensen
Danish Coastal Authority

LUND
UNIVERSITY

Division of Water Resources Engineering
Lund University
Box 118
221 00 Lund, Sweden

Water Resources Engineering
TVVR 20/5013
ISSN 1101-9824

Lund 2020
www.tvrl.lth.se

Master Thesis
Division of Water Resources Engineering
Lund University

English title:	Beach Nourishment at Faxe Ladeplads in Zealand, Denmark - Evaluation and Assessment of Morphological Evolution
Swedish title:	Strandfodring vid Faxe Ladeplads på Själland, Danmark - Utvärdering av morfologisk utveckling
Author:	Anna Adell
Supervisors:	Björn Almström, Magnus Larson, Per Sørensen
Examiner:	Hans Hanson
Language:	English
Year:	2020
Keywords:	Beach nourishment, erosion, coastal protection, coastal morphology, sediment dynamics

Acknowledgements

This master thesis project has been conducted as the final form of examination to mark the end of my engineering studies at Lund University. I would like to thank my supervisors Björn Almström and Magnus Larson at the Division of Water Resources Engineering who have been enthusiastic, helpful and supportive of me throughout the process. The project was conducted in collaboration with the Danish Coastal Authority and I want to thank my supervisor Per Sørensen there. He always supplied expertise and knowledge regarding the project and showed great interest in my progress.

The field measurements which are presented as a part of the project were made possible by a great team and the data was a precondition for me to be able to complete the study. Thanks to Henrik Vinge Karlsson, Britt Gadsbølle Larsen and Nikolai Sørensen from the Danish Coastal Authority and Aart Kroon and Mikkel Fruergaard from the University of Copenhagen for a nice field day at Faxe. In addition I would like to thank Åsa Wallin at the institution of Geology at Lund University for guidance and assistance in the laboratory.

During the course of the project I have relied on data collection through numerous sources. It has been very developing to engage with people in so many different roles. I would like to thank Poul Jensen at the Municipality of Faxe who happily supplied data and photo documentation. I would like to thank the staff at the Agency of Data Supply and Efficiency for their great collaboration in assisting with metadata of the orthophotos used in the study. I would like to thank Klaus Renholds at Faxe Kalk A/S who showed great interest in my project and supplied much useful information and previous reports. I also want to thank my best friend Malin Jansson for producing some of the illustrations presented in the report.

Finally, I want to express my deepest gratitude and appreciation to everyone that made my studies in Lund so special and memorable.

Abstract

The recent beach nourishment performed at Faxe Ladeplads in Zealand, Denmark was established with the objective to reduce wave overtopping onto the adjacent road and also aimed to restore a beach for recreation. During the time that the nourishment has been in place, the appearance of the beach has changed significantly compared to when it was initially restored. This project focused on studying the morphological evolution of the nourishment in the recent time that it has been in place. The study aimed to increase the knowledge of the sediment dynamics in the area and identify governing mechanisms for the changed appearance. The study found indications of nourished material being transported via longshore drift and depositing in the area downdrift the location of the nourished area. In addition, the nourished area and restored beach seem to be greatly impacted by lee side erosion that occurs as an effect of the close proximity to the nearby harbour. This phenomenon was recorded to impact the coastal area even before the nourishment was established, however the effect appears to be more pronounced since there is now additional material present in the system. To combat the issues of lee side erosion, it is suggested that a more active bypass operation that sources material on the updrift side of the harbour pier is further investigated.

Contents

1 Introduction

1.1 Background

Recently, there has been a nourishment action performed in Faxe Ladeplads in the eastern part of Zealand, Denmark. The objective of the nourishment was to primarily reduce wave overtopping onto the adjacent road, *Strandvejen*, and secondly to create a beach for recreation (Ramboll, 2016a). The initial nourishment took place in the fall of 2018. A volume of 62,000 m^3 (Danish Coastal Authority, 2017b) of sand was then distributed evenly along the coastal stretch between the harbour and the outlet of Faxe Creek located downdrift the harbour (Ramboll, 2016a), a distance of 630 m (COWI, 2013). In the project proposal, presented by Ramboll (2017), it was additionally stated that maintenance nourishment of 15,000 – 20,000 m^3 is to take place every fifth year, to maintain the size of the beach. This is an estimated amount and it is stated that the volume of material needed for maintenance nourishment should be continuously evaluated as it may vary dependent on storm impact (Ramboll, 2017). However, in the recent period that the nourishment has been in place, the appearance of the beach changed quite drastically. In addition, it appears that the rate of erosion varies along the coastal stretch where the initial nourishment was placed. To optimize the maintenance nourishment it is important to carefully identify the dominant sediment transport pathways and the magnitude of these, which may have been governing the morphological evolution of the nourishment.

Performing nourishment in areas where hard coastal protection structures are in place is an appropriate action to reduce the erosion pressure on the structure while also limiting wave overtopping on to infrastructure. Beach nourishment is a so-called nature-based solution for coastal protection, which more resembles a natural system and is dynamic in its characteristics (Dean & Rosati, 2009). Therefore, it is often required to perform consistent maintenance after the initial nourishment. In some cases, beach nourishment may be combined with dredging operations as a source of nourishment material, an operation commonly denoted bypass.

1.2 Objective and Research Questions

The objective of the project is to study the morphological evolution of the nourishment and evaluate the performance with respect to beach width. The morphological evolution will be studied along with wave climate conditions to estimate if the wave climate has been typical during the period since the initial nourishment action. Through data analysis and modelling, the aim is to identify sediment movement of the nourishment material in order to estimate which sediment transport pathways and mechanisms have been governing for the evolution of the nourishment. In order to fulfill the objective of the thesis the following research questions will be answered:

- How much material has been lost from the profile since the initial nourishment?

- Are there any indications of transport of nourishment material in the longshore and cross-shore directions?
- Is it possible to identify any sediment transport mechanisms that has played a significant role in governing the evolution of the nourishment?

Answering the research questions will enable for the formulation of potential site specific recommendations to apply in order to optimize future maintenance nourishment. In addition, a general objective of the project is to increase the knowledge of nourishment dynamics and impact in areas where conditions are similar.

1.3 Methodology

1.3.1 Literature Review

The documentation related to the coastal protection action is relatively abundant and in the form of project reports presented by Ramboll and permits granted by The Danish Coastal Authority. In addition, previous projects conducted in the area are available from various consultancy firms, which present the conditions and development of the area. This material is considered to present an extensive literature review that focuses on details of the recent nourishment action and the conditions in the area, as well as relevant theoretical background regarding coastal processes. International as well as Swedish and Danish literature has been considered in the literature study.

1.3.2 Available Data

Available data to be used for the analysis include hindcasted wave data (wave height, wave period and wave direction) and water level data for the period July 2005 to March 2020, provided by The Danish Meteorological Institute (DMI). Historical orthophotos are available for download through The Danish Map Supply (Agency for Data Supply and Efficiency, n.d.). In addition, documentation regarding the nourishment consist of profile surveys conducted by the Municipality of Faxe shortly after the nourishment was established. The Danish Coastal Authority has photo documentation of the nourishment during the period that it has been in place.

1.3.3 Field Measurements

Field measurements were carried out as a part of the project, to generate material to account for recent changes of the nourished area. Field measurements included beach profile surveys, collection of sand samples and documentation through drone footage. The profile survey was conducted by using RTK-GPS equipment. Sediment samples were collected and analysed by sieving in the laboratory at the Institution of Geology at Lund University.

1.3.4 Data Analysis

Various suitable tools are used to complete the analysis. To study the morphological changes based on the profile surveys, MorphAn version 1.7.3, a tool morphological analysis developed by Deltares (2016) is used. The shoreline evolution is studied in available orthophotos, and analysed in ArcGIS. The ArcGIS extension software Digital Shoreline Analysis System (DSAS) version 5.0, developed by United States Geological Survey (USGS) (Himmelstoss, Henderson, Kratzmann, & Farris, 2018), is used to estimate rates of change.

1.3.5 Numerical Modelling

The nearshore wave transformation model EBED (Mase, 2001) is applied to study the nearshore wave fields in the area around the harbour and nourished area. The rate of potential net longshore transport is estimated based on calculations according to the CERC-formula (U.S. Army Crops of Engineers, 1984). Both annual and monthly variations are studied.

1.4 Report Disposition

Chapter 2 of the report, presents the relevant theoretical background for the project where emphasis is put on sediment transport processes, coastal morphology and coastal protection. In Chapter 3, details regarding the study site in terms of conditions and historical development is presented. The details of the recent nourishment action are provided as well.

Chapter 4 provide information of the conducted field measurements, the procedure and equipment used is described in detail. The result and finding based on the field investigation are presented and discussed in the subsequent section, Chapter 5.

Chapter 6 presents the details of the conducted shoreline evolution analysis. The methodology and theory behind the used tools are presented, followed by a presentation of the results with corresponding discussion. In the next chapter, Chapter 7, the numerical modelling procedure is presented, along with the obtained results. Chapter 8 provide a summary of key discussion points to frame the findings of the study leading up to the final Chapter 9 in which the conclusions and recommendations of the project are presented.

2 Coastal Processes

2.1 The Coastal Zone

The coastal zone is composed of several separate zones, each individually defined. As the characteristics and processes varies between the zones it is important to study them separately. Figure 2.1 shows how the coastal zone is composed of several smaller zones presented along with the correct terminology used to describe the coastal zone. Located the furthest away from the coast is the offshore zone which is characterized by that the sediment transport induced by waves is insignificant (Davidson-Arnott, 2010). The larger portion of wave induced sediment transport occur in the littoral zone. This zone is dominated by significant coupling between the waves and the sea bed. The littoral zone is divided in to nearshore zone and beach/shore zone. The beach zone consist of the backshore and the foreshore zone. The backshore stretches from the coastline to the shoreline and this is the portion of the beach which is impacted by waves during storms (Davidson-Arnott, 2010). In the backshore area, berms are commonly present, which is an elevation of the sandbank. Several berm crests on a beach indicates exposure of a recent storm, with different elevations corresponding to the impact of different water levels. During storm conditions, large waves erode the berm and transport the material offshore (U.S. Army Crops of Engineers, 1984). In the offshore direction, the backshore zone is followed by the foreshore zone. This area of the coastal zone is impacted by waves in calm conditions (Davidson-Arnott, 2010). The part of the foreshore zone where wave runup on the beach occur is called the swash zone. Then follows the surf zone which is the zone of broken waves. Properties that affect wave breaking are beach slope and wave height. Hence, the location and stretch of this zone will vary depending on the conditions at any given beach at any given time (Davidson-Arnott, 2010).

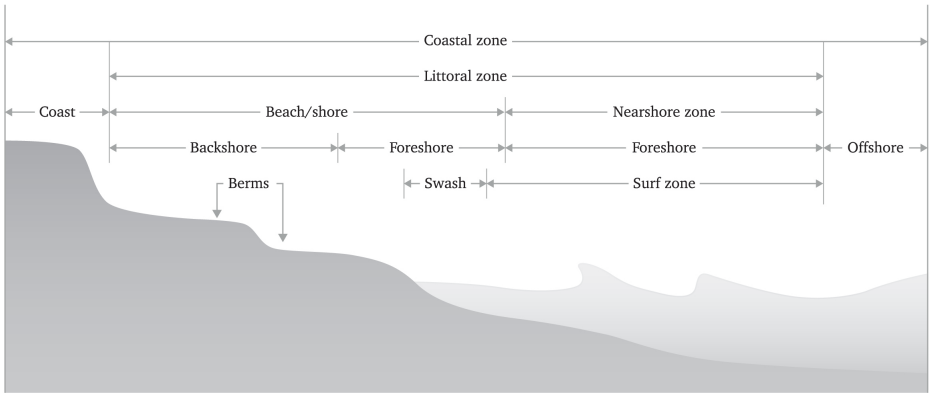

Figure 2.1: The coastal zone. Illustration: Malin Jansson.

2.2 Waves

Waves contain energy that is dissipated at breaking. Due to the energy transformation that occurs in the nearshore region, waves have significant impact on coastal development and the forming of beaches (U.S. Army Crops of Engineers, 1984). In the nearshore region, waves supply energy which can transform the coastline as waves transport sediment to and away from the coast, causing erosion or deposition of sediment. Ocean waves are complex and irregular by nature and waves may interact, changing the course of propagation and other wave properties (U.S. Army Crops of Engineers, 1984). This makes it difficult to describe waves mathematically, simplifications are needed which potentially reduces the accuracy of calculation. The simplest form of wave theory is to approximate the wave profile of ocean waves by sinusoidal waves. This is applied in the *Airy Wave Theory*, which is a linear wave theory and hence the simplest form of wave theory (Davidson-Arnott, 2010).

2.2.1 Wave Characteristics

Figure 2.2 shows a simple schematic sketch of a sinusoidal wave, used to describe the characteristics of water waves. The highest point of the wave is called wave crest and the lowest point of the of the wave is called wave trough. The wave height, H is defined as the vertical distance between a wave crest and wave trough. The distance between two wave crests (or two wave troughs) is defined as the wave length, L. The time it takes for a wave to travel the distance equal to one wave length is defined as the wave period, T. The wave celerity, C is the speed at which a wave travels, and is given by the relationship between the three parameters is given by Eq. 2.1 (U.S. Army Crops of Engineers, 1984).

$$C = \frac{L}{T} \tag{2.1}$$

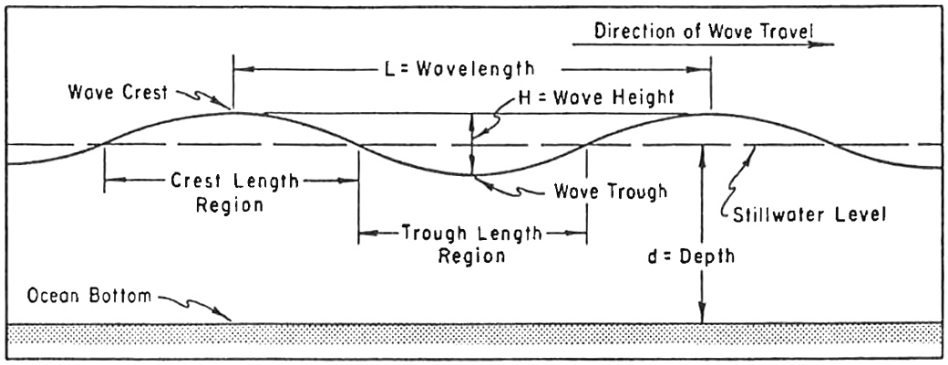

Figure 2.2: Definition sketch of wave characteristics (U.S. Army Crops of Engineers, 1984).

A real wave record is more complex than the wave presented in Figure 2.2. However, a complex wave form may be described by a series of different sinusoidal waves, to represent varying amplitudes, phases and frequencies. Performing spectral analysis on the wave record decomposes the complex wave form to several sinusoidal waves (Davidson-Arnott, 2010).

A real wave record contains waves that vary in height and period, these may be analysed according to the zero-upcrossing or zero-downcrossing method (Fig. 2.3). The method is used to define the wave heights and corresponding periods represented in the wave record. Once identified, the characteristics of H and T may be used to derive statistics that represent the wave record. The statistics will not vary between the zero-upcrossing method or zero-downcrossing method, it is rather a difference in the definition of the wave. The *significant wave height*, H_s corresponds to the average of one third (1/3) of the largest waves and may be extracted from the wave statistics. The significant wave height provides a common way to define and represent the wave heights in a record (Davidson-Arnott, 2010). The significant wave height is approximately equal to the spectral significant wave height, denoted H_{m0}, which is the denotation further used in this report.

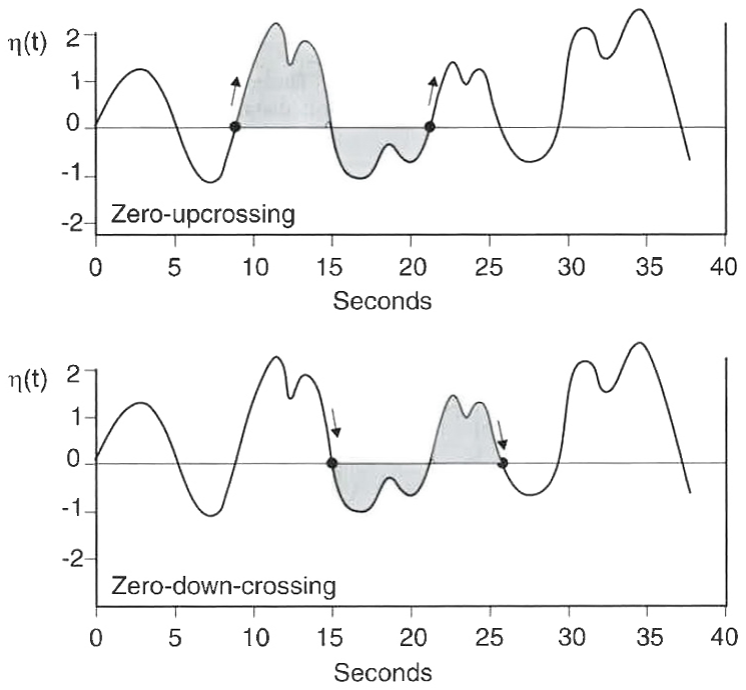

Figure 2.3: Zero-upcrossing and zero-downcrossing method for analysis of waves, (Davidson-Arnott, 2010).

2.2.2 Classification of Waves

Waves are classified dependent on the ratio between water depth, d, and wave length, L. Dependent of the magnitude the d/L-ratio, waves are categorised either as deep water waves ($d/L > 0.5$), transitional waves ($0.04 < d/L < 0.5$) or shallow water waves ($d/L < 0.04$) (U.S. Army Crops of Engineers, 1984). The d/L-ratio provides a measure of the interaction between the wave and the sea bottom. This implies that when the ratio is greater that 0.5 the wave characteristics are independent of water depth, while at a ratio smaller than 0.04 the wave characteristics are highly influenced by the bottom.

2.2.3 Wave Transformation

The definition of wave celerity provided by Eq. 2.1 may be further developed to give an expression for wave celerity, C as a function including the water depth, d and the gravitational constant g:

$$C = \frac{gT}{2\pi}\tanh\left(\frac{2\pi d}{L}\right) \tag{2.2}$$

As a wave progresses towards the shore, the water depth decreases and the interaction between waves and the sea bottom increases, this phenomenon is known as *shoaling*. This interaction will generate changes in the wave properties of wave length, celerity, height, direction and shape (Davidson-Arnott, 2010). As the wave progresses to shallower water depth, the wave height increases, the wave period remains constant, the wave celerity decreases and hence must the wave length also decrease proportionally. The formation of the sea bed will be governing the properties of waves as they approach the shoreline. The wave crests will align with the bottom contours and result in bending of the wave, induced by that the part of the wave in deeper water will move faster than the part of the wave in shallower water (U.S. Army Crops of Engineers, 1984). This bending phenomenon is known as *refraction* and is generated as an effect of the variation of wave celerity along the wave crest. Refraction and shoaling simultaneously impact the wave height of a progressing wave.

As a wave progresses in shoaling water, the wave steepness (H/L) will increase which cause wave *breaking*. The steepness increases due to shoaling which drives an increase in wave height and a decrease in wave length and celerity. The height at which a wave breaks, i.e. the breaking wave height is denoted H_b. Studies have found that the depth at which the wave breaks (h_b) is slightly greater that the breaking wave height. The relationship between the breaking wave height and the breaking depth is given by Eq. 2.3. (Davidson-Arnott, 2010).

$$\frac{H_b}{h_b} = 0.78 \tag{2.3}$$

Waves that approach and hit natural or man-made obstacles located in the coastal zone, such as a small island or a harbour construction, can cause different types of wave transformation. For example, *diffraction* of waves which is a phenomenon commonly detected if progressive waves hit an object. The wave energy is then transported laterally along the wave crest, causing the wave to bend around the structure. Diffraction generates changes in the wave height and form behind the structure. Waves may also *reflect* as they hit an object in the coastal zone. When waves are reflected it is the wave energy that is either fully or partially reflected. Potential reflection is important to consider in the construction of e.g. harbours and other structures in the coastal zone. (Davidson-Arnott, 2010).

2.3 Currents

Currents are an important mechanism for circulation in the nearshore zone. Currents are generated due to a variety of processes, creating a difference in water elevation. For example, currents can be generated as an effect of tide, wind and wave breaking on a beach. The difference in water elevation cause water to flow from areas of higher water elevation to areas of lower elevation, and this generates a current. Currents are an important component of sediment transport in the nearshore zone. Two common types of currents present in the nearshore zone are *longshore currents* and *rip currents*. A longshore current is a current directed parallel to the coast. They are created in shallow water when waves approach the coast at an angle. Rips are currents directed perpendicular to the shore. They arise due to the seaward motion of return transport of water brought to the beach zone by wave action. (U.S. Army Crops of Engineers, 1984).

2.4 Sediment Transport

Sediment transport is the process through which coastal sediments are moved in the nearshore region, induced by waves and currents. Sediment transport include processes that transport sediments both perpendicular (cross-shore) and parallel (longshore) to the shore. These are commonly treated separately as their impact on the net sediment transport in the coastal area is evident at different time scales (Davidson-Arnott, 2010). Transport of coastal sediments by waves and currents, in the nearshore region, drive either erosion or deposition of sediments and leads to changes in the coastal profile. The *depth of closure*, or depth of active (sediment) movement marks the depth at which there is no longer any exchange of sediments between the nearshore and the offshore. Beyond the depth of closure there is no significant change in bottom morphology (Kraus, Larson, & Wise, 1998).

It is common to distinguish between three different transport modes of sediment transport, namely *bed load*, *suspended load* and *sheet flow*. Bed load transport occur in close approximation of the sea bed. During bed load transport, moving grains are in constant contact with the bed (Fredsøe & Deigaard, 1992). For motion to occur, the bed shear stress must exceed a threshold of motion which is related to the

sediment grain properties. Suspended load refers to sediments being transported in suspension throughout the water column. In contrary to bed load transport, grains moving in suspension have no contact with the bed. In the sheet flow transport mode, grains are transported in several layers as bed load (Fredsøe & Deigaard, 1992).

Depending on the grain size, different transport mechanisms will be governing the process (Davidson-Arnott, 2010) and dominate the transport mode. Fine sediments, i.e. silt and clay, are transported in suspension in the water column but are only able to deposit in calm water conditions (Davidson-Arnott, 2010). Whereas coarser sediments, i.e. sand and gravel, typically are transported as bed load transport.

2.4.1 Longshore Sediment Transport

Longshore sediment transport refers to transportation that runs parallel to the shoreline. Longshore sediment transport is due to wave action generating wave motions and longshore currents. When waves break, sediment is put in suspension and transported due to wave energy in the alongshore direction. Breaking waves also induce a longshore current which also transports sediment. The rate and direction of the longshore transport is dependent on wave properties, including angle of approach, wave energy and duration. Thereby, the longshore sediment transport rate varies on both an hourly, daily and seasonal scale. (U.S. Army Crops of Engineers, 1984)

In coastal engineering practices, it is important to differentiate between gross and net longshore sediment transport. This is due to the variability in the direction and rate of longshore transport induced by varying wave properties. As indicated by Eq. 2.4 below, the gross transport rate, Q_G corresponds to the sum of the transport rates in both left and right directions, Q_L and Q_R (Davidson-Arnott, 2010).

$$Q_G = Q_L + Q_R \tag{2.4}$$

The net transport rate however is the transport rate in a predefined direction as it is defined as the difference between the leftward and rightward according to Eq. 2.5 (Davidson-Arnott, 2010).

$$Q_N = Q_L - Q_R \tag{2.5}$$

Regimes of sediment transport quantities and directions are crucial to understand the dynamics in an area of interest. The net sediment transport rate can be applied to predict the shoreline evolution of an open coastline. While estimates of gross transport rates are important for planning and maintaining dredging operations. For example, erosion or accretion of material adjacent to structures in the coastal zone is a noticeable effect and indication of net transport, while gross transport impact siltation of navigation channels. (Davidson-Arnott, 2010).

2.4.2 Cross-shore Sediment Transport

Sediment transport in the on-offshore direction is commonly denoted cross-shore transport, and occurs in direction perpendicular to the shoreline. Offshore transport dominates periods with intense storms while calm conditions typically experience onshore transport. (Davidson-Arnott, 2010). These types of short-term, seasonal differences in the conditions generate natural changes in the beach morphology. Storm waves erode the beach and transport the material offshore, where it deposits and builds up as sand bars. During calmer periods, the beach recovers and cross-shore transport is in the onshore direction. The material from the bars is transported back onto the beach plane. Thereby, over a longer time period, of months or years, this drives the cross-shore transport to reach equilibrium and has limited long-term effects on the beach (Davidson-Arnott, 2010).

2.4.3 Sediment Sorting

Shoaling and wave breaking increase the wave asymmetry, i.e. peaked crest and shallow trough. Wave asymmetry is the main governing process that influences sediment sorting in the cross-shore profile due to velocity differences under the crests and troughs, respectively. Under a passing wave crest the velocity has onshore direction while under a passing wave trough, the velocity is in the offshore direction. In addition, the velocity under the wave crest is higher compared to under the wave trough. This typically cause larger sediment grain sizes to move onshore while finer sediments are transported offshore. (Hassan, 2003).

Studies of sediment sorting in the cross-shore direction have found a clear trend in the variation of grain size along the cross-shore profile. The coarsest material in the profile is typically found in the swash zone. From this point, the median grain size d_{50} generally decreases in both the landward and seaward direction (Hassan, 2003). The finest material in the dry beach profile are typically the aeolian deposits, found in the dunes (Hallin, Almström, Larson, & Hanson, 2019). Regarding variation of grain size in the longshore direction, Hallin et al. (2019) discovered that the median grain size decreased significantly in the direction of the longshore drift. This phenomenon may be specific to the investigated study site as the study by Hallin et al. (2019) also presented a nearly unidirectional longshore sediment transport. Hence suggesting that longshore sediment sorting is highly dependent on the local conditions.

2.4.4 Sediment Budgets

A sediment budget formulated for a specific time frame and section of the coastline compiles long-term information regarding sediment sources and sinks, as well as rates and directions of transport. Setting up a sediment budget for a specific site aims to identify various pathways of sediment transport and the magnitude of these. Inputs and outputs of sediments to the coastal area can be either natural, or arise from various man-made activities such as dredging or artificial nourishment.

Natural sediment sources are for example river influx and sea-cliff erosion, while sediment sinks are for example wind transport of sediment. (Rosati, 2005).

To formulate a sediment budget for a specific coastal area, the coastal area is commonly divided into multiple control volumes, or cells, and the sediment transport patterns for each specific cell are studied individually. The calculations consider all possible sources Q_{source} and sinks Q_{sink} of sediment. The difference between sources and sinks must be equal to the change of sediment volume in the area, when engineering activities have been accounted for. Algebraically this is expressed by the relationship provided in Eq. 2.6

$$\sum Q_{\text{source}} - \sum Q_{\text{sink}} - \Delta V + P - R = Residual \tag{2.6}$$

where ΔV is the net volume change within the cell, P and R represent any engineering activities causing sediments to be added or removed artificially. *Residual* thereby represents the level at which a cell is balanced, i.e. a balanced cell is equal to zero (Rosati, 2005). This enables estimations whether a coastal area is suffering erosion or if there is accretion of sediment material. Sediment budgets are an important tool in coastal zone management as it displays transport dynamics for the system. The information compiled in a sediment budget enables planning and managing coastal activities, and may by studied for example to estimate future rates of erosion or accretion of sediment (Rosati, 2005).

2.5 Morphological Changes

2.5.1 Coastal Erosion

Coastal erosion is permanent loss of beach material from a coastal system. Coastal erosion is highly dependent on processes related to weather conditions (e.g. wave climate and storm surges) and beach properties (e.g. slope, sediment composition) (van Rijn, 2011). During storm conditions severe coastal erosion can occur. However, it is important to highlight other potential causes as well, including both natural and man-made causes (U.S. Army Crops of Engineers, 1984). Sea level rise can cause of coastal erosion. Increase of the surface elevation drives coastline profile changes and results in long-term retreat of the coastline. Sediment is naturally supplied to the coast though rivers and longshore sediment transport. Variations of sediment supply through these processes result in beach erosion (U.S. Army Crops of Engineers, 1984). Human activities in the coastal area, such as the construction of harbours and marinas, have been proven to cause coastal erosion. Even coastal protection structures, with the objective to reduce erosion can lead to increased coastal erosion further downdrift the structure (van Rijn, 2011). Coastal erosion can be classified into chronic erosion and acute erosion. Chronic beach erosion is long-term erosion which occurs in the time-frame over several years or decades. It is driven by variations in the longshore sediment transport and marks the erosion potential of a coastal area. Acute erosion occur due to simultaneous

high water levels and large wave impact, for example during storm events. It occurs on relatively few occasions, even with years apart, but cause dramatic changes of the beach morphology and cause great retrieval of the coastline (Danish Coastal Authority, 2016).

2.5.2 Coastal Variability

It is important to differentiate between coastal erosion, which is permanent loss of beach sediments, and natural coastal variability. Shoreline variations occur due to fluctuations in the amount of beach material (van Rijn, 2011). A beach system is dynamic and will change with the seasons due to the impact of external factors. This generates characteristic seasonal variations which may be identified as reoccurring summer and winter profiles. During the summer season, when wave conditions are calm, a beach with a wide berm and a more steep profile is formed. Whereas, a winter profile is typically less steep due to the impact of waves with higher energy and storm conditions are more common (Komar, 1998). During storms, large waves erode the beach berm and transport the material offshore. This causes the beach width to decrease and generates the formation of sand bars in the nearshore zone (U.S. Army Crops of Engineers, 1984). During calm conditions the beach is able to recover and the bars typically migrate onshore again. Storms can cause distinct and rapid changes of the beach profile. Figure 2.4 shows the natural seasonal variation of the coastal profile. Short term variations of the shore profile occur due to seasonal climate changes and wave, tide and storm surge conditions (Stive et al., 2002).

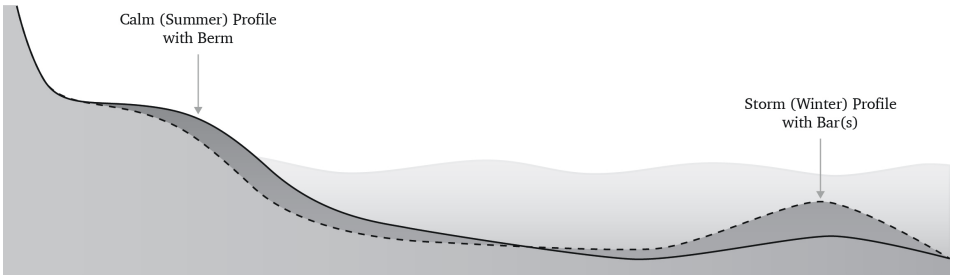

Figure 2.4: Seasonal variation of the coastal profile. Illustration: Malin Jansson.

The slope of the beach profile is highly correlated with the size of sediment grains. Coarser sediments give a steeper profile and finer sediments give a more gentle profile (Davidson-Arnott, 2010). The sorting of sediments along the beach profile is governed by wave asymmetry as well as sediment properties, such as density and grain size. The sorting process which occur due to wave asymmetry caused by wave shoaling results in coarse sediments being transported onshore while finer

sediments are transported offshore. This causes the slope to gradually decrease in the offshore direction (Davidson-Arnott, 2010).

2.6 Coastal Protection

2.6.1 Beach Nourishment

An eroding coast is sediment deficient. Hence, if it is desired to limit retreat of the coastline, sand must be supplied artificially. Beach nourishment is a form of coastal protection action, where large quantities of sand is placed in the nearshore area and in the subaerial part of the beach (Dean & Rosati, 2009). Beach nourishment is a so-called nature-based solution for coastal protection that more resembles the natural system and is dynamic in its characteristics (Dean & Rosati, 2009). The nourishment can reduce the rate of erosion but not cease the problem should the coast be sediment deficient, which is the case for eroding coasts. Therefore, it is often required to regularly perform maintenance nourishment after the initial protection is in place. Performing artificial nourishment in areas where hard coastal protection structures are present is an appropriate action to reduce the erosion adjacent to the structure, while also limiting wave overtopping on infrastructure. The nourishment provide a gentler slope in front of the structure which reduces the height of breaking waves and hence limits the rate of overtopping. Coastal protection through beach nourishment have proven to yield numerous positive effects, in addition to erosion protection, such as increased recreational value, storm protection and positive ecological effects (Dean & Rosati, 2009).

There are different types of artificial nourishment to apply depending on characteristics of the coastal area and also the objective of the coastal protection. *Shoreface nourishment* is a method where nourishment material is placed offshore, typically at the seaward side of the outer bar. Sand is deposited offshore, from boats which makes the method reasonably cheap. The method increases the amount of sand in the nearshore zone and relies on natural processes to nourish the beach long-term. Shoreface nourishment requires relatively large volumes of material, as approximately only 20-30 % will reach the beach zone in a period of 5 years (van Rijn, 2011). Shoreface nourishments have both longshore and cross-shore effects that impact the coastal processes in a way that causes sediment to be trapped in the nearshore zone. The offshore placement of the material will cause large waves to break at the seaward side of the nourishment which generates a decrease of longshore transport in the landward direction. At the same time onshore transport is increased due to wave asymmetry of shoaling waves passing the nourishment. (van Rijn, 2011).

Another method are *beachfills* which are commonly applied as a type beach restoration. The objective is often to compensate for local erosion or to restore the recreational value of a beach. Some requirements for beachfill nourishments include that the beach slope should not be too steep and ideally the fill material used is typically slightly coarser than the native material. Finer material can give extensive

losses and therefore requires larger volumes to be used as compensation. The method requires pumping of sediment though a pipe from an offshore location to the beach face, which is quite costly. Furthermore, the method may be limited by the availability of suitable source material in a nearby location. The life-time for beachfills is roughly 1-5 years depending of the type of coast, but the nourishment is highly impacted by local storm conditions and maintenance is required regularly to maintain the beach width. (van Rijn, 2011)

2.6.2 Coastal Protection in Denmark

Denmark is a relatively small country, with an area of approximately 43,000 m^3 making up one large peninsula (Jutland) and about 500 islands, of which 200 are inhabited. This gives the country a geography that resembles a large archipelago (Sørensen, Fredsøe, & Roed-Jakobsen, 1996). The Danish coastline is consequently very long, about 8750 km (DR, 2014). The west coast of Jutland is most exposed and vulnerable and has an estimated erosion rate of up to 4 m/yr. Here, and in other parts of the country the need for coastal protection and management is considerable. Climate change is also expected to impact the state of Danish coasts, caused by sea level rise, storm surges, extreme rainfall and coastal erosion (Faragò, Rasmussen, Fryd, Rønde-Nielsen, & Arnbjerg-Nielsen, 2018).

A study conducted by Faragò et al. (2018) aimed to map the historical and recent coastal protection strategies in Denmark. The study found that historically, hard coastal protection solutions, such as dikes or sluices were widely used. To protect against coastal erosion, groynes and breakwaters were commonly applied. The study found that the recent (from year 2000) coastal protection strategies against storm surges and sea level rise include hard coastal protection solutions; dikes, seawalls and sluices. Strategies to combat coastal erosion include sand nourishment, wave breakers and groynes. Additionally, the authors identified that practice to design multi-purpose solutions had seen an increase in recent years. This is achieved by, for example, designing solutions that focuses on combining coastal protection with recreation and aesthetic values. (Faragò et al., 2018).

In general, the responsibility to perform coastal protection falls on the landowner, who thereby is responsible for applying for permission, building and maintaining the installation and also cover all related expenses. However, the government will engage in the construction and operation if the coastal protection is considered to be of national importance (Danish Coastal Authority, n.d.). The Danish Coastal Authority is the official government organisation, responsible for authorizing permits for coastal protection and any other construction in the coastal zone.

3 Description of Study Area

3.1 Site Location

The *Inner Danish coasts* is the collective term used to define all the Danish coasts other than the North Sea coast. They account for the majority of the total length of Danish coasts, and conditions are very diverse. The inner Danish coasts are typically categorised into three different types of coasts; (1) Northern coasts along Kattegat with medium exposure, (2) eastern and southern medium exposed coasts in the Baltic and (3) all other coasts along fjords, straits, belts and sheltered islands with low exposure. (Sørensen et al., 1996).

Denmark is a county of islands, and Zealand is the largest of the Danish islands, which hosts the capital city Copenhagen. Located 60 kilometers south of Copenhagen, in the southeastern part of Zealand there is a small coastal town called Faxe Ladeplads (Figure 3.1). It is located approximately in the middle of Faxe Bay, placed in the southwestern part of the Baltic Sea.

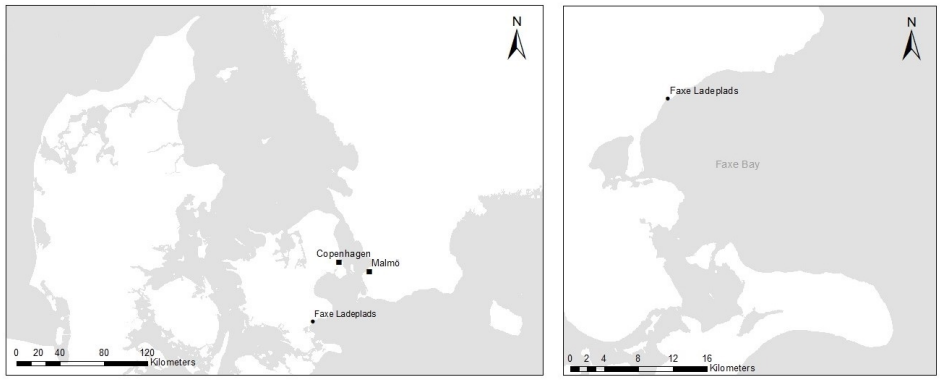

Figure 3.1: Geographic Location of Faxe Ladeplads.

In Faxe Ladeplads there is a harbour and an operating marina, which enables both shipping, leisure sailing and fishing. Faxe has a large limestone quarry and the industry connected to it is of great importance for the community. The company Faxe Kalk A/S specialises in lime and chalk products used in a variety of industries and businesses, including agriculture and construction. Historically the lime from Faxe has been used when decorating many traditional Danish churches in the eastern part of Zealand. The construction of the harbour played a central role in the expansion of the lime business in Faxe as it provided extended routs of export (Aasbjerg, 2002). Figure 3.2 presents a map of the area, where the current layout of the harbour is clearly shown. Figure 3.3 presents a picture of the marina and the harbour, the northern part of the beach is also shown.

Figure 3.2: Close up view of the harbour and coastline at Faxe Ladeplads. WMS basemap from the Agency for Data Supply and Efficiency (n.d.) - Webservice liste (DTK/Skærmkort daempet).

Figure 3.3: North view of the marina and the harbour. The road Strandvejen and the northern part to the beach is also shown. Photo: Danish Coastal Authority, 2020.

The stretch of coastline downdrift the harbour, shown in Figure 3.2, is the main subject of this study. Figure 3.2 also shows the road Strandvejen which follows the coastline closely. This is the main road, connecting Faxe Ladeplads to other towns further south and inland. The beach area close to the harbour was once popular amongst visiting tourists as well as local inhabitants. However, the beach has successively eroded, leaving the road exposed. There has also been reoccurring events of wave overtopping and damage caused to Strandvejen during storms with large waves. To combat the problems with overtopping and erosion, and with an aim to reclaim the lost beach, a beach nourishment was carried out in 2018. The initial nourishment was placed in the area between the harbour and the outlet of Faxe Creek. There is a small groyne placed before the outlet of Faxe Creek (see Figure 3.4) and furthermore, there is a rock revetment placed adjacent to the road.

Figure 3.4: The groyne placed at the south end of the beach and just before the outlet of Faxe Creek. Photo: Danish Coastal Authority, 2020.

3.2 Bathymetry and Geology

Faxe Bay is located in the southwestern part of the Baltic Sea. The bay is confined by the headland of Stevns Klint to the north and Møn peninsula to the south (Kabuth & Kroon, 2013). Faxe Bay is surrounded by a sand coastline (Danish Coastal Authority, 2020) and the seabed sediments in the bay consist of mainly

sand, muddy sand and till (Geological Survey of Denmark and Greenland (GEUS), 2014). Figure 3.5a shows the geological composition of the seabed sediments in Faxe Bay.

Figure 3.5b presents a map of the bathymetry of the bay. At the end where the bay is open towards the rest of the Baltic Sea, the maximum water depth is 24 m. The bay has deeper sections that stretch along the headlands but generally gets shallower inside the bay.

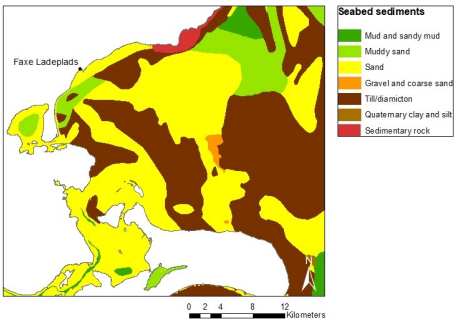

(a) Geological composition of seabed sediments (Map produced based on source data from GEUS (2020), Seabed sediment map.)

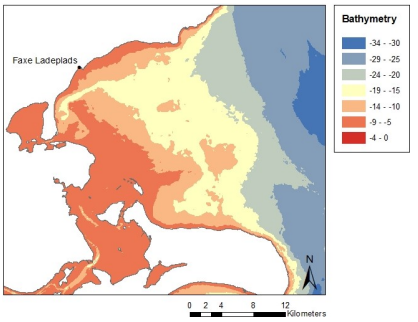

(b) Bathymetry of Faxe Bay. (Map produced based on source data from GEUS (2020), Height and Depth maps.)

Figure 3.5: Geology and bathymetry of Faxe Bay.

3.3 Wave Climate

The wave rose in Figure 3.6 presents the long-term wave climate during the period July 2005 to March 2020. Model data has been delivered by DMI and is generated from their hindcast model. The wave height is given as significant wave height (H_{m0}) at coordinates 55.210 N 12.183 E (water depth of 10 m). The data series also contain records of peak wave period (T_p) and incoming wave direction (θ). The data is used to produce the wave rose in Figure 3.6, which indicates that wave heights of 0-1 meters are the most frequent and the largest waves approach lie in the direction 110-120°, corresponding to approximately SE to ESE.

Figure 3.7 presents a map of the fetch lengths. The wave rose in Figure 3.6 indicates that the largest wave heights are generated at directions 100-120°, which may be explained by that the largest fetch lengths are in these directions.

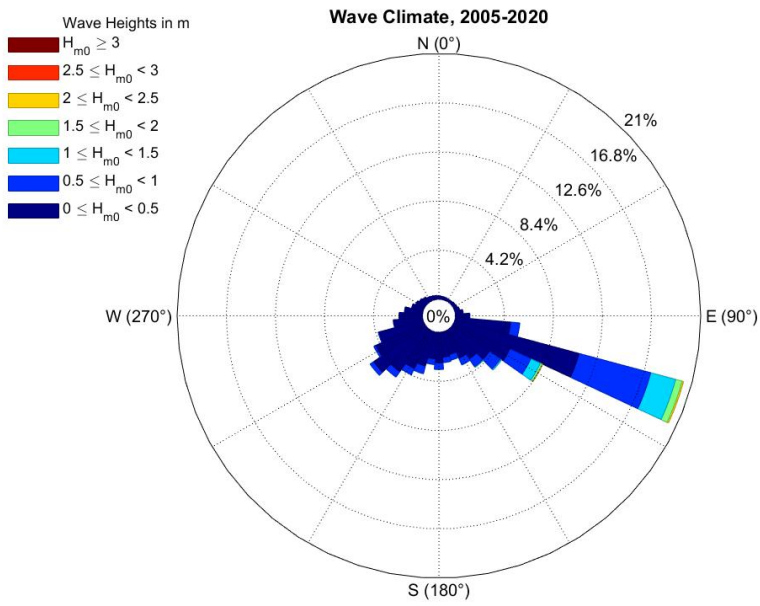

Figure 3.6: Wave rose indicating the wave climate produced with data from the period 2005-2020.

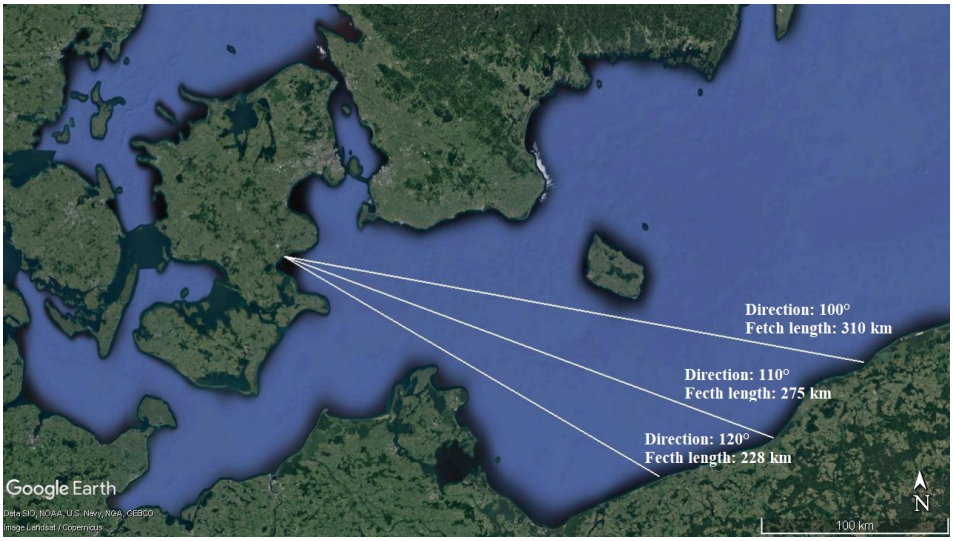

Figure 3.7: Fetch length map. (Graphics: Google Earth Pro, 2020.)

Figure 3.8 shows the computed monthly average significant wave heights for the period July 2005 to March 2020. A yearly average for the significant wave height is 0.35 meters. Based on the results presented in the bar diagram, it is possible to see that during six months of the year (October-March) the monthly average wave height is larger than average while during the remaining six months (April-September) the wave height is smaller than average. It is thereby evident that the wave climate is characterized by one period of the year with more waves of larger wave heights and one period when the conditions are calmer.

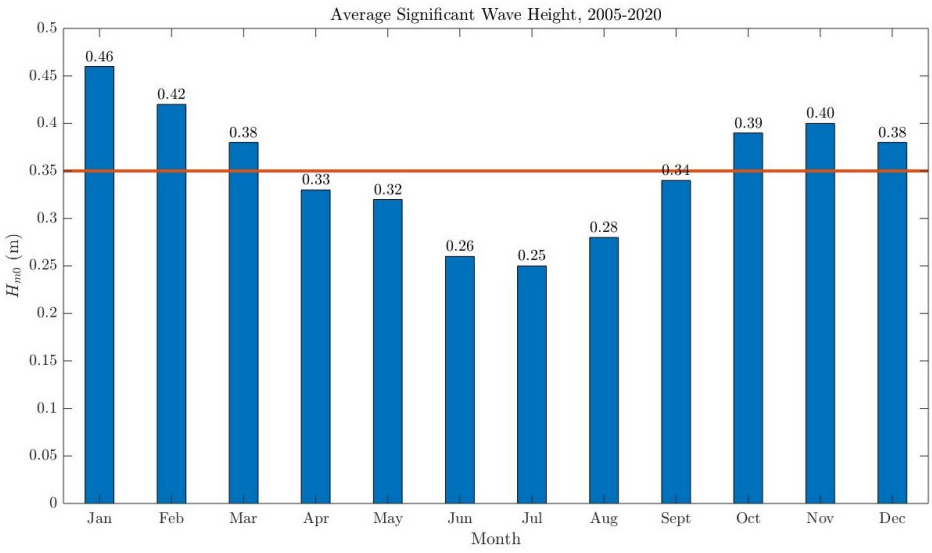

Figure 3.8: Monthly average significant wave heights, 2005-2020. The line represents the overall yearly average significant wave height of 0.35 m.

The maximum wave heights of each year during the data period (July 2005 - March 2020) are presented in Table 3.1. The data presented in Table 3.1 shows that the largest annual waves are generated during the period October-March, previously identified as the period with generally stormier conditions. This is true for all years except for 2005, when the largest wave is recorded in July. However, one potential explanation is that 2005 represents a shorter time period. Data is only available for July-December and consequently the remaining months are not represented. Furthermore, the data presented in Table 3.1 suggests that at least once a year, a significant wave height of about 2 meters is attained.

Table 3.1: Maximum significant wave height, H_{m0} (m), each year.

max H_{m0}	**Date**	**Year**
1.67	4-Jul	2005
1.55	5-Jan	2006
2.29	21-Feb	2007
2.04	4-Jan	2008
2.12	4-Nov	2009
2.34	2-Dec	2010
2.17	15-Feb	2011
2.38	23-Dec	2012
2.9	18-Mar	2013
2.73	19-Jan	2014
2.36	6-Oct	2015
2.14	15-Oct	2016
1.46	11-Jan	2017
1.41	15-Jan	2018
1.4	15-Nov	2019
1.52	9-Feb	2020

3.4 Water Level

Faxe Bay is located in an area where tidal fluctuations are insignificant. However, the inner Danish coasts can experience water levels of about ± 100 cm that are induced by storm surges due to strong winds (Baden & Aarosiin-Hansen, 2017). Figure 3.9 presents a scatter plot of significant wave height and water level for 2016, which represents an average year. The plot indicates that extreme waves only occur at high water levels, while high water levels can occur without extreme waves. High water levels in the southern Baltic Sea are caused by winds from north and east (Hanson & Larson, 2008). Due to the location of Faxe Bay, there are no waves generated at northerly winds. Easterly winds however, generate waves in combination with high water levels.

Currents are not very common in this part of the Baltic Sea. The currents that do occur are wind generated and mainly on the surface. It is estimated that they are not strong enough to transport sediment. The sediment transport is therefore thought to be governed predominantly by wave impact. (Ramboll, 2016b).

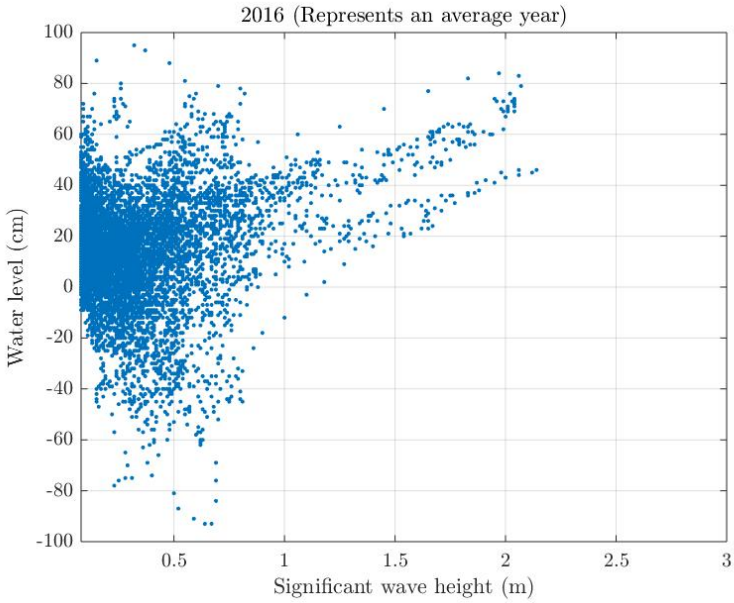

Figure 3.9: Significant wave height and water level for an average year (2016). The relationship shows that large waves coincide with high water levels, however high water levels occur without extreme waves.

3.5 Sediment Transport

The predominant direction of the net sediment transport in the area is towards the south. This is mainly due to the direction of the incoming waves and the orientation of the coastline (Mangor, Fuchs, & Rand, 2010). However, considerable transport in the northward direction has been recorded in periods with southerly winds (Baden & Aarosiin-Hansen, 2017). The sediment transport is also impacted by the layout of the harbour. The proximity of the harbour cause the transport mechanisms in the northern end of the beach to be rather complex (Ramboll, 2017). As an effect of that the predominant direction of sediment transport is from north to south along the coast, large amounts of sediment material deposits on the north side of the harbour pier (Mangor et al., 2010). In addition, it is a problem of siltation of the harbour's navigation channel which has to be dredged several times per year. The large accumulation of material is caused by the formation of a vortex in the southward current as it passes the upstream groin and enters the shallow and calm waters south of the harbour (Baden & Aarosiin-Hansen, 2017). The dredged material is composed of a mixture of sand and seaweed. Data of dredged volumes for a number of relatively recent years are presented in Table 3.2. A permit is granted that allows the dredged material to be deposited at an offshore location in Faxe Bay (The Danish Environmental Protection Agency, 2017).

Table 3.2: Dredged volumes.

2013	24,250 m^3 [1]	2017	19,170 m^3 [2]
2014	20,680 m^3 [1]	2018	23,984 m^3 [2]
2015	20,580 m^3 [1]	2019	22,520 m^3 [2]

[1] (Ramboll, 2016b), [2].

The dredged volumes provide an indication of the magnitude of the gross sediment transport in the area. The complex conditions with transport in altering directions, makes it complicated to set up an accurate sediment budget along coastline (Baden & Aarosiin-Hansen, 2017).

The Danish Coastal Authority (2016) classified the exposure level to be high and the acute erosion in the area around Faxe Ladeplads to be moderately high. The depth of closure in Faxe Bay is -4 meters (Danish Coastal Authority, 2016).

[2]Jesper Olsen, Harbour Master, Port of Faxe Ladeplads, email contact 24 April 2020.

3.6 Historic Development of the Harbour

The bedrock in the area around Faxe Ladeplads consists of limestone and established export of limestone dates back hundreds of years (Aasbjerg, 2002). The historical development of the coastline has been largely influenced by these activities (Mangor et al., 2010). A historical map of the coast (Fig. 3.10), from 1834, shows the four initial shipping locations; Vemmetofte, Jomfruens Egede, Rosendal and Lindesvold. At this time there was no harbour or pier constructed to facilitate the shipping. Instead the loading of goods on to the ships occurred out at sea, assisted by barges. (Aasbjerg, 2002). In this time, when the coast was not developed, the map in Figure 3.10 shows that the initial coastline was more or less straight (Mangor et al., 2010).

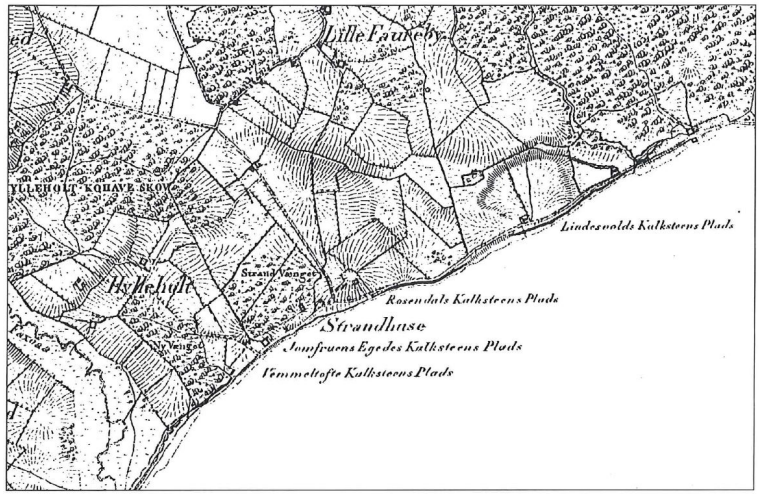

Figure 3.10: Map from 1834 showing the initial formation of the coastline (Aasbjerg, 2002).

The first pier was constructed in 1843, which made it possible for large ships to anchor at the pier where they could be loaded with goods. This pier was continuously extended during the 1850's to reach out at larger depths. A few years after, a second pier was built a bit further up the coast. However, the impact of winds and waves still made it impossible for ships to approach the pier at times. The two piers were thereby replaced by proper port facilities, complete with breakwaters, in 1864 and 1870 respectively. This solved the issue of wave impact by providing shelter from waves. Figure 3.11 shows the plan view of the two ports. The one constructed in 1864 was the largest one, and the one built in 1870 was at a larger water depth, but referred to as the 'small port'. Just a few years after construction, the two ports were severely damaged during the great storm of 1872. Significant repairs were required before they could operate again. (Aasbjerg, 2002).

Figure 3.11: Plan view of the two ports, noted which respective year they were constructed (Aasbjerg, 2002).

Another storm affected the area in late December 1904. It is unclear how significant the damages were to the harbour, however photos in Figure 3.12 show the damages caused to the coast just south of the harbour. Both the photos are taken so that they overlook the coastline with a northern view, and the harbour is visible in the background. The photos in Figure 3.12 show that the coastline was natural and unprotected at this time. i.e. in the beginning of the 20th century.

Figure 3.12: Photos showing the damages caused to the coastal area south of the harbour, during a winter storm in 1904, Left: (arkiv.dk, n.d.-b), Right: (arkiv.dk, n.d.-a).

The two ports were constructed without consideration of the sediment transport patterns in the area. Due to the southward direction of the sediment transport, accumulation of sediment material occurred in the gap between the two ports. As

regularly clearing the area through dredging was an expensive operation, the gap was eventually just left to fill up (Ramboll, 2016b). The disruption of the natural sediment transport also resulted in accretion of material on the updrift side of the small port whilst erosion occurred on the downdrift side of the larger port (Mangor et al., 2010). This caused the port to assume the shape that is indicated in Figure 3.13, it clearly shows how the coastline has advanced up until today.

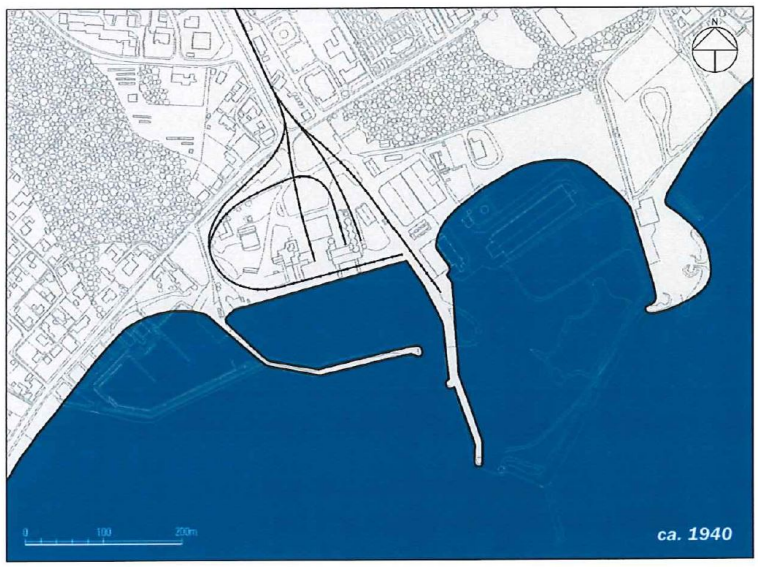

Figure 3.13: Appearance of the port around 1940, coastline advanced due to the sediment transport (Aasbjerg, 2002).

Due to the continuous problem with accumulation of material in the area between the two ports, the gap was instead filled up completely and the land was reclaimed. The land area extends 500 meters away from the initial coastline and has a complementary 80 meter long pier at the southern tip. Additionally, in 1985 the harbour was extended with a marina, specifically for leisure sailing and fishing (Mangor et al., 2010). Figure 3.14 presents a map of the harbour in 2002, and the design has remained the same to this day.

Figure 3.14: Map showing the current layout of the harbour which has remained since 2002 (Aasbjerg, 2002).

3.7 Coastal Protection in the Area

The coastline surrounding Faxe Ladeplads is subject to chronic erosion. The construction and development of the harbours along with other activities in the coastal area, during the 20th century, affected the sediment flow and increased the erosion. Groynes placed along the coast south of the harbour helped to reduce the problems with erosion (Ramboll, n.d.). Studies of historic aerial photos available at Danmarks Miljøportal (2020), show that groynes were more or less a permanent element of coastal protection during the majority of the 20th century. Figure 3.15 presents a photography from the 1960's where the placement of the groynes is clearly shown. The relatively significant beach width suggests that the groynes were effective at trapping sediment. In the photo, it is also possible to see the concrete wall protecting the adjacent road Strandvejen. Faxe Ladeplads was once a very popular tourist destination (Baden & Aarosiin-Hansen, 2017), and the photo showcases a vibrant atmosphere.

Figure 3.15: Photo from the 1960's, showing Strandvejen and the groynes placed along the beach south of the harbour (Mangor, Fuchs, & Rand, 2010).

In the early 2000's the groynes were severely worn down and as an effect their impact was significantly reduced. The groynes were ultimately removed but since then the beach gradually disappeared, only to leave the road Strandvejen exposed (Baden & Aarosiin-Hansen, 2017). In addition, there was a reoccurring problem with wave overtopping onto Strandvejen during storm conditions. During one particular storm in 2002 large amounts of sand and gravel washed up onto the road. As a cause of action, a rock revetment was constructed in 2003, with the objective to protect the road. Complementary to the revetment structure, a small artificial beach was established as well. Due to economic constraints, the original project plan did not include the establishment of a beach, but a limited amount of sand (1,200 m^3) was provided by Faxe Kalk A/S at a small cost. Figure 3.16 presents a picture from 2003 and shows a view of the established rock revetment along with a narrow beach strip in front of the structure. This material was not eroded as quickly as expected, and the beach was reasonably well maintained until 2005. In the years that followed the remaining sand eroded quickly and in 2008 the beach had completely disappeared (COWI, 2013).

Figure 3.16: Picture from 2003, showing the recently established rock revetment along with a narrow beach strip, (COWI, 2013).

3.8 Beach Nourishment Performed in 2018

In the fall of 2018 an artificial nourishment was carried out in Faxe Ladeplads. The initial nourishment was placed in the area between the harbour and the outlet of Faxe creek (Ramboll, 2016b), a stretch that is about 630 m long (COWI, 2013). The project proposal presented by Ramboll (2017) stated that the objective of the nourishment was to primarily reduce wave overtopping onto the adjacent road, Strandvejen, and secondly to create a beach for recreation. The reclaimed beach had a width of 20 meters. News reports from the time provide the impression that the action was very well received by the public. In interviews the local inhabitants expressed that they were excited about the fact that their town would once again have a beautiful beach of their own (Lundbye, 2018).

Figure 3.17 shows aerial photos of the beach area from August 2018, i.e. just months before the initial nourishment was carried out. In Figure 3.17a it is clearly shown that there is very limited material present and the rock revetment by Strandvejen is fully exposed. Figure 3.17b shows that the beach width increases a bit towards the groyne placed before the outlet of Faxe Creek.

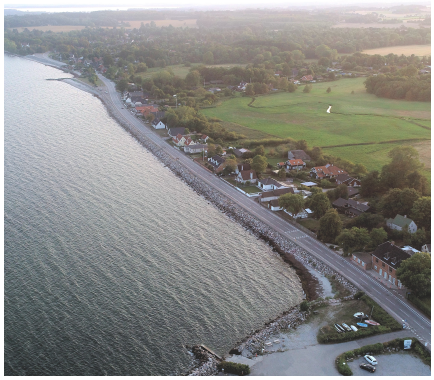

(a) South view. 16 August 2018.

(b) North view. 16 August 2018.

Figure 3.17: Aerial photos showing the beach before the initial nourishment. Photo: Danish Coastal Authority, 2018.

In the fall of 2018 the initial nourishment took place (Faxe Municipality, 2019). The Danish Coastal Authority had granted a volume 62,000 m^3 (Danish Coastal Authority, 2017b) of sand to make up the initial nourishment. Material for the initial nourishment was sourced offshore and pumped in a large pipe to enable the establishment of the beach. The native material has the grain size of $d_{50} = 0.1 - 0.2$ mm and this result is based on samples collected close to the harbour entrance and the navigation channel (Ramboll, 2016a). The median grain size of the fill material was slightly coarser compared to the native material, i.e. $d_{50} = 0.3$ mm. Using material with a median grain size of 0.3 mm was said to generate a nice beach for recreation (Ramboll, 2017) and meet the general recommendation that nourishment material is coarser than the native material. The nourishment was a beachfill nourishment. The beach slope from the foot of the rock revetment to the shoreline was 1:30 to progress to a gentler slope of 1:50 from the shoreline and 85-127 meters in the seaward direction (Ramboll, 2017).

Figure 3.18 shows an aerial view of the reclaimed beach, in December 2018, i.e. just after the nourishment was in place. The even width of the established beach is clearly shown in the figures. In Figure 3.18a it is also possible to detect a large amount of seaweed that has gathered at the end of the beach where it connects to the harbour. This is a common recurrence at Faxe Ladeplads and the municipality regularly performs maintenance by removing the seaweed from the area (Faxe Municipality, 2019).

(a) South view. 20 December 2018. (b) North view. 20 December 2018.

Figure 3.18: Aerial photos showing the beach after the initial nourishment. Photo: Danish Coastal Authority, 2018.

The project proposal, presented by Ramboll (2017), states that maintenance nourishment of 15,000 – 20,000 m^3 is to take place every fifth year. This corresponds to an approximate amount of 3,000 – 4,000 m^3 of material lost from the nourished area annually. This is an estimated amount and it is stated that the volume of material needed for maintenance nourishment should be continuously evaluated as it may vary dependent on storm impact (Ramboll, 2017). However, the shape of the beach has changed dramatically compared to when it was initially restored. It appears that the erosion rate is varying along the coastal stretch. This can potentially be because the harbour is limiting the longshore sediment transport, which is predominant from north to south (Ramboll, 2017).

The Danish Coastal Authority granted a bypass solution allowing dredged material from the navigation channel to be used for maintenance nourishment (Danish Coastal Authority, 2017a). The permit covers annual volumes of approximately 4000 m^3 of clean dredged material to be placed in two different locations. The first location is the same area where the initial nourishment was placed, and one additional location in the nearshore facing half of the beach and extends until the small groyne (Danish Coastal Authority, 2017a). A bypass solution provides a beneficial alternative for both maintenance of the coastal protection and maintenance the port and navigation channel. However, the dredged material is a mixture of sand, mud and seaweed and hence only a fraction of the quantities presented in Table 3.2 is of adequate quality to be used for maintenance nourishment. Data of dredged volumes in the recent years show that the content of clean material suitable for nourishment were 120 m^3 in 2018 and 420 m^3 in 2019 [2]. The quantities of clean material are hence not sufficient to make up the volumes of estimated annual loss of nourishment material.

[2]Jesper Olsen, Harbour Master, Port of Faxe Ladeplads, email contact 24 April 2020.

4 Field Measurements

Field measurements were conducted at the site in Faxe Ladeplads on 3 March 2020. The purpose of the field measurements was to collect additional data to be used for analysis and modelling. The field study included collection of sand samples, profile measurements and aerial documentation by drone footage. The area for investigation consisted of the stretch of the coastline between the harbour and the outlet of Faxe Creek, i.e the area where the initial nourishment was placed. In addition, an area north of the harbour as well as the coastline south of the outlet of Faxe Creek were included for investigation. The areas are from here on referred to as 'North', 'Beach' and 'South'.

4.1 Collection of Sand Samples

Sand samples were collected to perform analysis of sediment grain size distribution. Along each sampling cross-shore profile, samples were collected at seven specific sampling points. Figure 4.1 show a schematic image of the placement of the sampling points. The sampling points in the beach profile include aeolian deposits (a), two separate samples in the backshore (b & c), a reference point located between the swash zone and the beach berm (d), the swash zone (e), one sample at 0.6 m depth and 1.0 m depth (f & g).

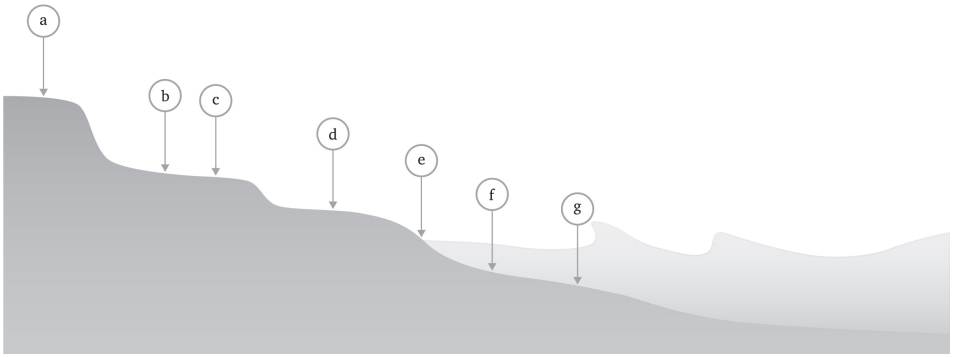

Figure 4.1: Location of sampling points along the cross-shore profile. Illustration: Malin Jansson.

The point located halfway between the swash zone and the berm crest is a common reference point for sediment sampling. Narra, Coelho, and Fonseca (2015) found that the median grain size (d_{50}) at this point is representative for the entire beach profile and displays relatively limited variation. Thereby, sampling at this point yield results that is comparable between profiles.

Ten separate profiles were selected to collect the sediment samples; two sampling profiles north of the harbour, six sampling profiles along the nourished area and two

sampling profiles south of the outlet of Faxe Creek. Figure 4.2 shows the location of the ten sampling profiles, color coded to display the three different areas. Exact coordinates are provided in Appendix. Samples collected at the north side of the harbour, were thought to represent "native" conditions as the dominant direction of the sediment transport is southward directed (Mangor et al., 2010). The area south of the creek outlet is included for investigation to study if the grain size distribution in this area resembles the characteristics of the nourished area or the north area.

(a) Sampling profiles north of the harbour.

(b) Sampling profiles along the nourished area and south of the creek outlet.

Figure 4.2: Map showing the locations of the sampling profiles.

Dry samples were collected by using a metal beaker with a volume of 100 ml. Samples at points e, f, g, i.e. points located out in the water were collected by using a metal beaker attached to a wooden stick in order to reach down to the bed, the improvised device is shown in Figure 4.3.

Figure 4.3: Device used to collect nearshore samples, i.e. in the swash zone and at water depth 0.6 m and 1.0 m. Photo: Anna Adell, 2020.

Sediment analysis was carried out in the laboratory at the institution of Geology at Lund University (GeoCentrum). The sediment samples were dried in an oven at 105 degrees until fully dry, which took between 12-24 hours depending on the water content of the samples. For each sample, 200 grams of dry material was then analysed by sieving. The sieve set-up was made up by sieves with meshes 2, 1.4, 0.71, 0.5, 0.355, 0.25, 0.18, 0.125, 0.09 and 0.063 mm. The sieves plates were stacked in descending order and shaken automatically for 15 minutes. Thereafter, the weight of the material trapped at each respective disk was recorded. The results are presented and discussed in section 5.1.

4.2 Profile Measurements

A profile survey was conducted by using RTK-GPS equipment with the purpose to generate additional beach morphology data. A total of 35 individual profile lines were measured in the beach area where the initial nourishment had been placed, resulting in measurements approximately every 18 meters, see Figure 4.4a. These 35 lines had been identified and extracted from beach survey data from December 2018 (i.e. recently after the nourishment was in place) provided by the Municipality of Faxe. The area south of the creek outlet was also included for investigation. However, since this area lacked previous profile surveys, the measured profile lines were more generously spaced here. A total of six profile lines were measured in this area, see Figure 4.4b.

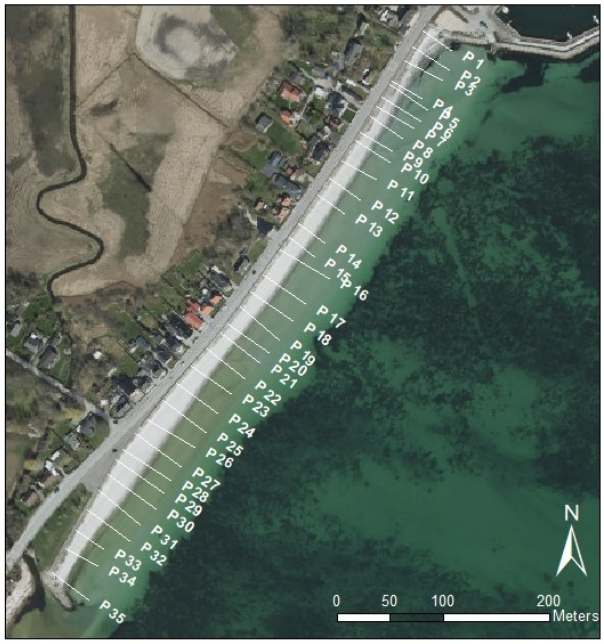

(a) Profile lines main beach (P1-35)

(b) Profile lines south (PS1-6)

Figure 4.4: Maps showing the locations profile lines measured on 3 March 2020.

Two instruments were used to conduct the survey which was divided into landward and seaward measurements. Figures 4.5 and 4.6 presents action shots of the survey being conducted. Seaward measurements were performed by people equipped with waders, see Figure 4.6. The landward measurements commenced at the top of the revetment adjacent to the road Strandvejen (see bottom left in Figure 4.5) and reached to the swash zone. The red and white stick visible in Figure 4.6 was used as an indicator to mark where the landward measurements ended and the seaward measurements began. This procedure assured that measured data was located along the same straight profile. The seaward measurements stretched approximately 30-60 meters out in the water depending on the water depth profile. During the day of the measurements the water level was recorded at +61 to 67 cm, which impacted how far out the profiles could be measured.

Figure 4.5: Action shot of the beach profile survey being conducted. Photo: Danish Coastal Authority, 2020.

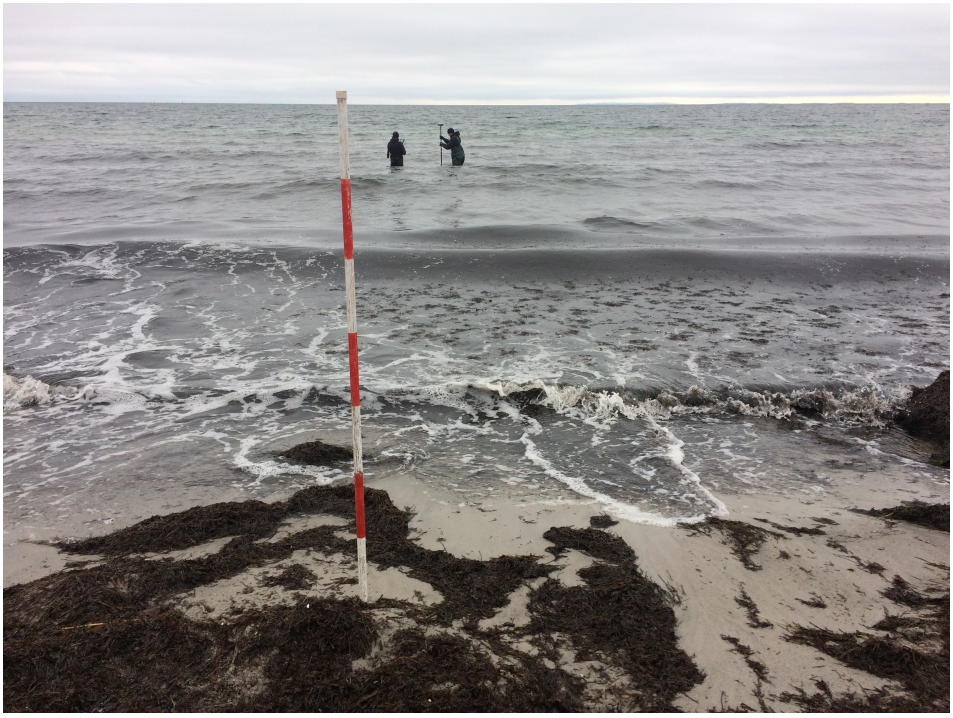

Figure 4.6: Procedure to conduct the seaward measurements. Photo: Anna Adell, 2020.

In addition, cross-shore profiles that reached further in the seaward direction were measured by boat and by using echo sound technology. However, due to certain circumstances this data could not be processed and analysed within the time frame of this project and is unfortunately not presented as a part of the report.

4.3 Additional Documentation

The Danish Coastal Authority were responsible for collecting documentation in the form of aerial photographs from UVA. The areas of interest, i.e. the nourished area, the are north of the harbour and the area south of the creek outlet, were separately investigated by collecting drone footage.

5 Results of Field Measurements

In this section results obtained from and derived from data gathered at the study site on 3 March 2020 are presented and findings are discussed. Details and complete data sets are provided in Appendix.

5.1 Grain Size Distribution Analysis

Based on the results of the sieve analysis, grain size distribution curves were derived. Figure 5.1 shows the grain size distribution curve of profile P15 which corresponds to a line located roughly in the middle of the nourished area. The remaining plots are attached in Appendix.

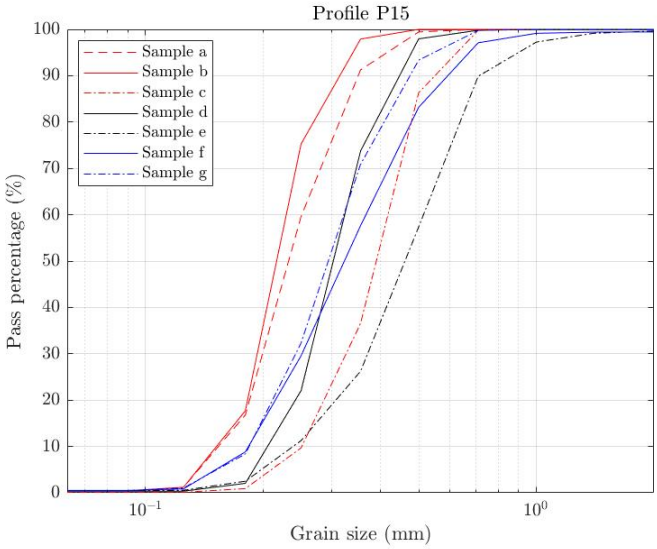

Figure 5.1: Grain size distribution curve for profile P15 to display an example.

From the grain size distribution curves it is possible to read the median grain size d_{50}, which corresponds to the grain size at a pass percentage of 50% in the grain size distribution curve. The results of d_{50} for each individual sample are presented in Table 5.1. Missing data indicates that no sample was collected at this point. This is due to the fact that the point could not be identified in the profile. For example, Figure 5.2 present a photo from the day when the field measurements were conducted. It shows a section of the coast along the nourished area where the dry beach plane had eroded and the rock revetment was exposed. Profile P21 was located in this area and hence the sampling was affected. The exception of the missing data, is sample PS4-e. This sample contained a lot of coarse elements ($d > 2$ mm) that was trapped at the top sieve, which hence made up the majority

of the sample weight. Consequently, it was not possible to determine d_{50} from the grain size distribution curve (see Appendix), according to the same method as for the other samples. The sample PS4-e is hence excluded, however it should be noted that the mean value of d_{50} for sample point e for the area 'South' should technically be slightly higher than presented in the following section.

Table 5.1: Median grain size d_{50} (mm) for all samples. PN corresponds to area 'North', P indicates area 'Beach' and PS is area 'South'.

	a	**b**	**c**	**d**	**e**	**f**	**g**
PN1	0.35	0.39	0.52	0.55	1.07	0.43	0.39
PN2	0.42	0.35	0.37	0.52	0.82	0.38	0.39
mean	**0.39**	**0.37**	**0.45**	**0.54**	**0.95**	**0.41**	**0.39**
P2	-	0.32	0.47	0.42	0.66	0.49	0.22
P11	0.27	0.32	0.27	0.27	0.28	0.31	0.23
P15	0.23	0.22	0.39	0.30	0.46	0.32	0.29
P21	0.27	-	-	-	0.54	0.26	0.22
P27	0.27	0.31	0.22	0.35	0.63	0.23	0.21
P34	0.39	0.42	0.28	0.39	0.58	0.36	-
mean	**0.29**	**0.32**	**0.33**	**0.35**	**0.52**	**0.33**	**0.24**
PS2	-	0.45	0.39	-	0.57	0.45	0.29
PS4	-	0.37	0.34	0.29	(-)	0.25	0.32
mean	-	**0.41**	**0.36**	**0.29**	**0.57**	**0.35**	**0.31**

Figure 5.2: Photo from 3 March 2020 showing a section of the coast where the beach had eroded all the way to the rock revetment. Photo: Danish Coastal Authority, 2020.

The results presented in Table 5.1 show that the median grain size of samples sourced in areas 'North' and 'South' are coarser than the native material of $d_{50} = 0.1 - 0.2$ mm. The d_{50} of the native material however was obtained from samples sourced at the harbour entrance and the navigation channel (Ramboll, 2016a) and at these locations the sediments are generally finer. This is due to that at larger water depths the conditions are calmer and there is less turbulence induced by wave action, which allows fine material to settle. The material in the beach plane however, is greatly impacted by wave action. Wave action cause finer material to be put in suspension which then may be transported offshore. This reduces the representation of the fine sediment grain sizes and causes the median grain size of beach and foreshore samples to be higher compared of offshore locations. The coarse material detected in areas 'North' and 'South' may be an effect of recent storm impact that removed great amounts of fine material available in the beach and foreshore area and hence generating a greater result of the median grain size. The result of median grain size in the area 'Beach' resembles the median grain size of the fill material used for the nourishment known to be $d_{50} = 0.3$ mm. This results implies that it is in fact fill material that is present in this area.

To present the results graphically, specific sampling points and profiles have been investigated separately, to map the variation in distribution along the coastline as well as along the cross-shore profile. Mean values and standard deviation for d_{50} in the specific sampling points have been computed for the three separate areas, 'North', 'Beach' and 'South' and the results are presented in Figure 5.3. The sampling points are presented in increasing cross-shore distance in the seaward direction, starting at the location of the aeolian deposits (at dune or rock revetment) and ending with the most seaward sampling point g at approximately 1.0 m depth.

Samples from profiles located in area 'Beach' (red circular markers in Figure 5.3) show the same generic trend as similar studies of sediment grain size distribution along a cross-shore profile (Guillen and Hoekstra, 1997; Narra et al., 2015). The coarsest material is found in the swash zone (sample e) followed by the reference point (sample d). From the swash zone the median grain size decreases in the seaward direction. The lowest median grain size for the profile is recorded in sample point g. From the reference point (sample point d), located half way between the swash zone and the berm crest, the median grain size is decreasing in the landward direction. The finest material in the dry part of the profile is recorded in sample point a which corresponds to aeolian deposits.

Samples from profiles in areas 'North' and 'South' also show this general trend in the cross-shore variation of median grain size, however with some deviating results in certain points. For example, for area 'North' the lowest mean median grain size was recorded in the beach plane (sample point b) and not in the aeolian deposits. While for area 'South', the reference point (sample point d) gave the lowest result of mean median grain size. It should however be noted that fewer samples were collected in areas 'North' and 'South' compared to area 'Beach'. Hence, the mean values of d_{50} for sample locations in areas 'North and "South' are obtained from

only 1-2 samples while the corresponding number is 5-6 samples in area 'Beach', see Table 5.1.

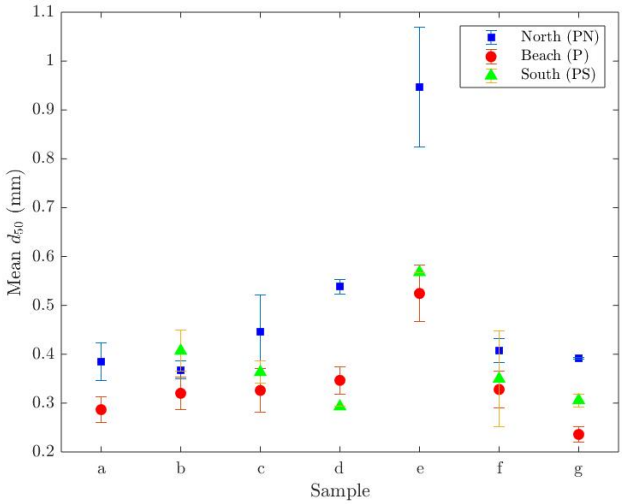

Figure 5.3: Variation of median grain size, d_{50}, in the three investigated areas.

The result presented in Figure 5.3 generally indicates that the samples sourced at location 'North' has a larger median grain size compared to locations 'South' and 'Beach'. This is true for all sampling points except point b where the highest mean d_{50} was found at location 'South'. This difference in d_{50} on either side of the harbour can indicate that there is limited exchange of material between the two locations. Which is probable as the dominant direction of net longshore transport is southward. It is thereby suggested that the material on the north side of the harbour can be considered to represent native characteristics and most likely has not been influenced by the nourishment. Furthermore, the finest sand is typically found at location 'Beach'. This is valid for all sampling points except point d where location 'South' displayed the finest result. It should however be noted that the result is based solely on one sample and should be questioned to represent the entire area. The mean d_{50} for the samples collected in area 'South' are typically in between the results for areas 'North' and 'Beach'. The result might be an effect of native coarser material available in area 'South' prior to the initial nourishment action, mixed with finer material from the nourished area.

The parameter d_{84}/d_{16} is a common measure used to evaluate the grain size sorting in a sample. The values of d_{84} and d_{16} correspond to the grain sizes at pass percentages 84% and 16%, respectively. The values were sourced from the grain size distribution curves corresponding to each individual sample, in the same manner as when determining d_{50}. The sorting parameter for all individual samples along with

computed mean values are presented in Table 5.2. A lower value of the sorting parameter indicates a narrower distribution of grain sizes in the sample.

Table 5.2: Sorting parameter d_{84}/d_{16} for all samples. A lower value represents a more well-sorted sample.

	a	**b**	**c**	**d**	**e**	**f**	**g**
PN1	1.71	1.80	1.91	1.71	3.52	3.32	2.41
PN2	2.26	1.80	1.91	1.94	3.44	2.33	2.28
mean	**1.99**	**1.80**	**1.91**	**1.82**	**3.48**	**2.83**	**2.35**
P2	-	1.91	1.85	1.65	5.35	2.75	1.88
P11	1.79	1.83	1.74	1.68	1.98	2.19	1.76
P15	1.85	1.65	1.81	1.81	2.39	2.53	2.17
P21	1.80	-	-	-	4.55	1.87	1.85
P27	1.94	1.82	1.80	1.76	2.55	3.09	2.02
P34	2.13	1.94	1.75	1.71	4.09	2.73	-
mean	**1.90**	**1.83**	**1.79**	**1.72**	**3.48**	**2.53**	**1.94**
PS2	-	2.07	1.70	-	2.33	2.50	1.92
PS4	-	1.90	1.81	1.91	(-)	3.76	2.38
mean	**-**	**1.99**	**1.76**	**1.91**	**2.33**	**3.13**	**2.15**

Typically the aeolian deposits are expected to display the most well-sorted result, with the lowest value of the sorting parameter d_{84}/d_{16}. However, this is not the case for the results presented in Table 5.2. Hence it is suggested that there has been some issues with sampling the aeolian deposits correctly. Due to the layout of the coastal area, the aeolian deposits were difficult to eliminate separately. Thereby the samples have potentially been contaminated by material that are not solely aeolian deposits. This can potentially explain why the obtained value of the sorting parameter for samples a does not display the most well-sorted results.

Figure 5.4 presents a graphic display of the variation of the sorting parameter d_{84}/d_{16} in the different areas. The result shows that the beach samples. i.e. sample points a-d are more well sorted compared to the remaining nearshore samples (samples e-g). The most seaward sample (sample g) has the lowest result of mean d_{84}/d_{16} of the nearshore samples, while the largest variation of grain sizes is typically found in the swash zone (sample e).

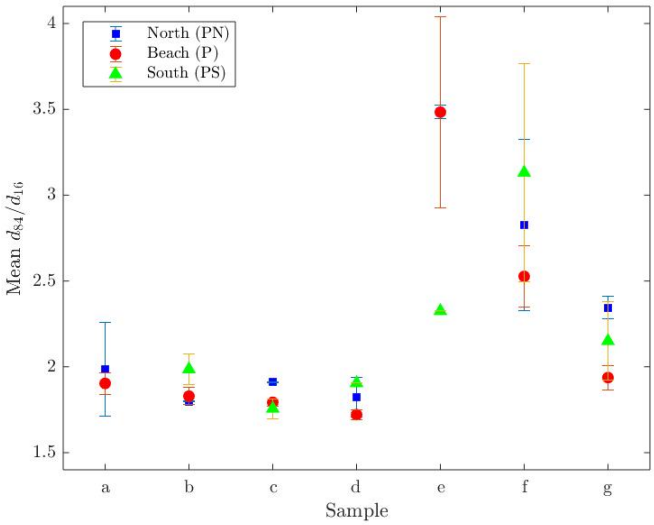

Figure 5.4: Variation of the sorting parameter, d_{84}/d_{16}, in the three investigated areas.

Figure 5.5 shows the results of median grain size d_{50} (top) and the grain size sorting parameter d_{84}/d_{16} (bottom) in sampling point d, for the profile lines PN1, PN2, P2, P11, P15, P27, P34 and PS4. No samples were collected at this point for profiles P21 and PS2. In the case of profile P21, a sample at this point could not be collected as the beach had been eroded all the way up to the revetment so the each plane was non-existing (see Fig. 5.2) and hence there was no berm crest to mark the upper limit to identify the reference point. PS2 displayed a complex profile and it was impossible to identify the reference point accurately. The result in Figure 5.5 shows that the median grain size is larger for the profiles in the area north of the harbour, compared to the other sampling locations. That there is a difference between the median grain sizes on either side of the harbour, could indicate that there is limited exchange of material. From profile P11 to P34 there is a steady increasing trend in median grain size. This can potentially be a result of increasing wave impact in the direction towards the groyne and reflects the direction of the longshore drift.

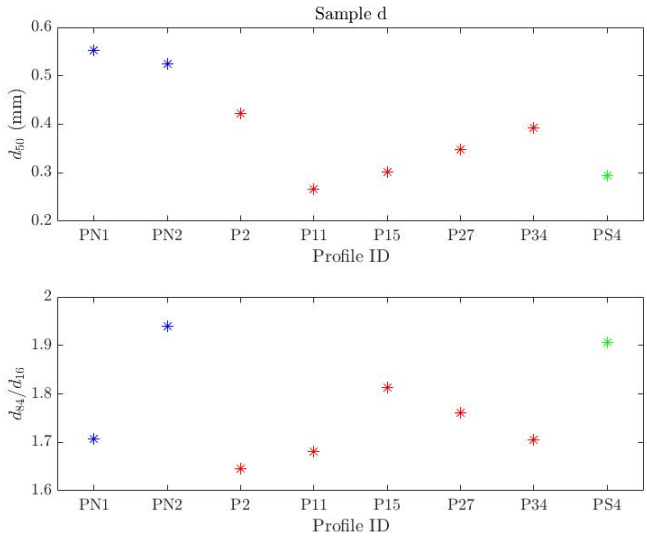

Figure 5.5: Results of d_{50} (top) in the reference point (sample point d) along with the sample's sorting parameter d_{84}/d_{16} (bottom).

Furthermore, the result in Figure 5.5 shows that the samples along the nourished area (P2, P11, P15, P27, P34) are typically more well-sorted compared to samples collected along profiles PN2 and PS4 as the ratio d_{84}/d_{16} is generally lower. Additionally, Figure 5.4 shows that the lowest mean value of the sorting parameter in sample point d is obtained for area 'Beach'. This can potentially be an effect of the homogeneous characteristics of the material used for the initial nourishment.

The result of d_{50} for sample point d in profile PS4, is of a magnitude that resembles the d_{50} obtained along profiles in area 'Beach'. This may indicate that it is in fact nourished material present in the profile, which is probable as the net longshore sediment transport is southward directed. This would suggest that material from the nourished area is transported past the groyne and deposits in the beach profile south of the creek outlet. It should however be noted that this estimation is based solely on one sample and may not be representative for the whole area 'South'.

Sources of Error

There are some potential sources of error related to the procedure of sampling and sieving analysis of sand samples to be pointed out. Firstly, for collecting surficial samples from the bed in the nearshore zone, i.e. sample points g and f, the improvised device was used (Fig. 4.3). When sampling with this method there is a possibility that the finest material is washed away and not represented in the sample, as the device is elevated through the water column to reach the surface. This can cause the content of fine grain sizes in the sample to be slightly

underestimated, and hence generate a higher result of median grain size, d_{50}. The results of d_{50} obtained for sampling points g and f are considered to still be adequate in relation to the other sampling points and hence it is not thought to compromise the result significantly. However, it is good to be aware of the limitations with the sampling method and that it might not be suitable to apply if more accuracy is desired.

Secondly, occasionally the summed weights for the grain sizes making up a sample, the result was slightly lower than the initial weight of the sample (200 grams). When conducting the sieving procedure, occasionally the amount of material trapped at a specific plate was so small that the weight was not detected by the scale. This phenomenon was especially noticeable for the bottom most plate, corresponding to grain sizes $d < 0.063$ mm. The scale precision was set to measure with a two decimal accuracy, which was considered to be sufficient for the purpose of the analysis. Control weighing the sample after sieving was conducted to assure that the initial sample weight was attained. The deviating result when summing the intermediate weights, corresponding to the respective grain sizes, is thereby probably an effect of the scale accuracy.

5.2 Results of Profile Measurements

Data from the profile measurements was analysed using the morphology analysis tool MorphAn developed by Deltares. MorphAn was used to plot cross sections of the measured profiles. Plots of the profile cross sections are presented in Figure 5.6 where the profile lines have been grouped together depending on distance from the harbour. The result shows that the profiles extend about 30-50 meters in the cross-shore direction. The plots showing the profiles of P19-P24 and P25-P30, show the tendency of a bar formed at approximately a cross-shore distance of 40-50 meters and a depth of 0.5 meters. This morphological feature is identified in the cross sections P16-P18 and P31-P32 as well, although it is not as easy to detect in combination with the additional profiles in the plot. It is possible that the bar is present in the profiles located closer to the harbour (P1-P15) as well, though the measurements did not extend past 40 meters in the cross-shore direction, which would cause the bar to not be included.

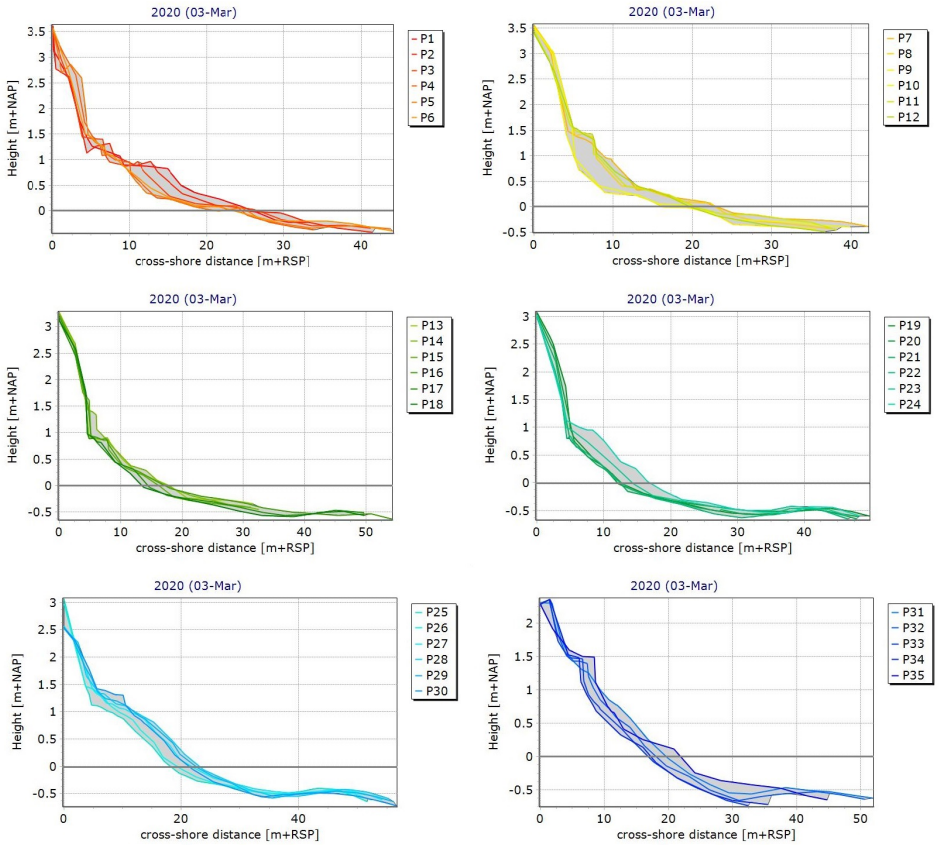

Figure 5.6: Profile cross-sections for profiles P1-35, from 3 March 2020.

Similarly, the profile cross sections measured in the area south of the outlet of Faxe Creek were plotted using MorphAn. In this area only six profile lines were measured and they are grouped together in one plot. The results are presented in Figure 5.7. The results show that the profile lines PS2, PS3 and PS4 extended much further in the cross-shore direction compared to PS1, PS5 and PS6, indicating that this area is much shallower. The shallow area identified in the area south of the creek outlet is an effect of continuous accretion and build-up of sediment. The appearance displayed in the three profiles is likely caused by material from the nourished area that has bypassed the groyne and deposited, resulting in a shallower area.

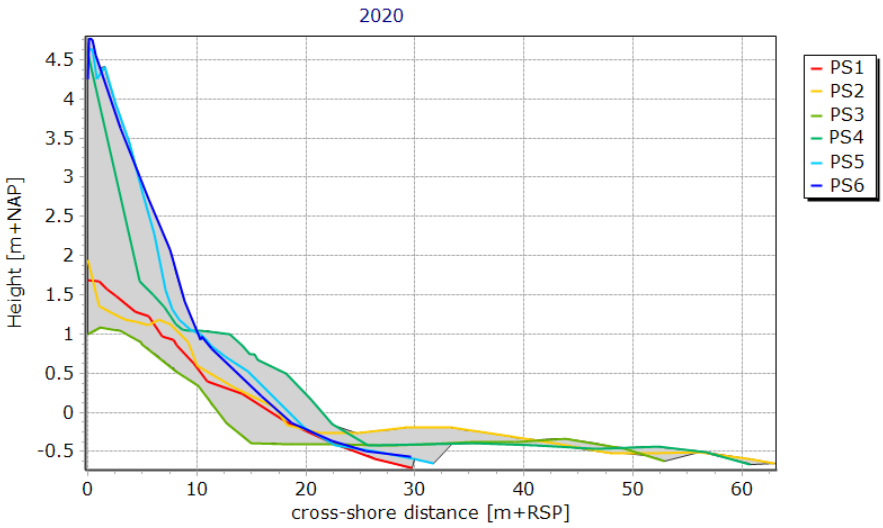

Figure 5.7: Profile cross-sections for profiles PS1-6, from March 3rd 2020.

5.3 Volume Calculations

A beach profile survey was conducted by the Municipality of Faxe in December 2018, i.e. recently after the nourishment was in place. Complementing data gathered during the field study on 3 March 2020 enabled for analysis of beach profile evolution of profiles P1-35. Data from these two different years were analysed to estimate the volumetric change.

The profile cross sections from 2018 and 2020 were analysed in the MorphAn Volume Development Model to estimate volumetric change. The model requires certain boundary conditions to be applied. The purpose of the boundary conditions is to assign the vertical and horizontal extent in order to confine the volume cross section to be calculated. The boundaries include, seaward and landward boundaries as well as upper and lower boundaries. The seaward and landward boundaries were set to default values. The default value for the seaward boundary corresponds to the most landward measurement between the profiles for the two separate years in the analysis. The default value for the landward boundary corresponds to the most seaward measurement between the profiles for the two separate years analysed. The cross-shore location of the measurement points will hence govern the horizontal extent at which the volume is calculated. The vertical boundaries were assigned based on the elevation data. The available profile surveys unfortunately do not extend all the way to the depth of closure. The analysis is restricted to only calculate the amount of material in the dry part of the profile. The upper limit was set to +2.0 meters which corresponds to a point located on the rock revetment, where no change is expected. The lower limit was set to 0.0 meters. The purpose

is to study the change in volume between the two separate beach survey events. The rock revetment contribute with a volume that is not sand, but also does not change between the two studied years. These boundary conditions are therefore considered to be the most appropriate to use for the purpose of the study, as the method studies relative volumes rather than absolute volumes.

Figure 5.8 presents an example of the output from the MorphAn volume development model, where the volume has been calculated for profile P7. The profile line from 2018 is however governing for the section to be calculated, so that the obtained result is comparable between the two studied years. The figure displays that the most landward measurement is located at a cross-shore distance of approximately 2 meters while the most seaward measurements is located at approximately 31 meters, which is the extent of the profile line from 2018. These hence define the landward and seaward boundaries, respectively. The orange sections in the plots in Figure 5.8 are thereby excluded from the volume.

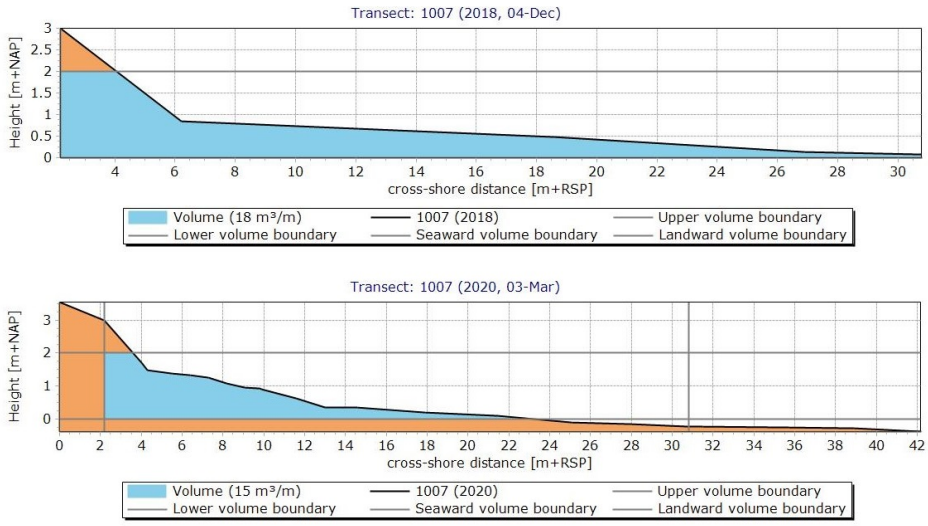

Figure 5.8: Profile sediment volumes for profile P7. Example display of MorphAn model output.

The tool computes the sediment volume present in the profile, for individual years. The result is given in the unit m^3/m, i.e. volume per meter of longshore distance. To calculate the volume, based on the MorphAn volume result was multiplied by a distance, perpendicular to the profile line. This yields a method where the coastal stretch is divided into segments, as presented by Figure 5.9. The profile is thereby assumed to represent the segment within the box it is located. The entire beach volume is calculated based on the profile volumes for all profiles located along the coastal stretch. Figure 5.9 presents a close up view to show how the boxes are defined. The length of the longshore distance is given by half the distance to the

neighbouring profiles. The method to define the perpendicular distances is inspired by a study conducted by Hanson (2013), that mapped sediment volume changes at a study site in Ystad, south of Sweden. The profile lines are placed quite closely, which generates the perpendicular distances of around 10-25 meters.

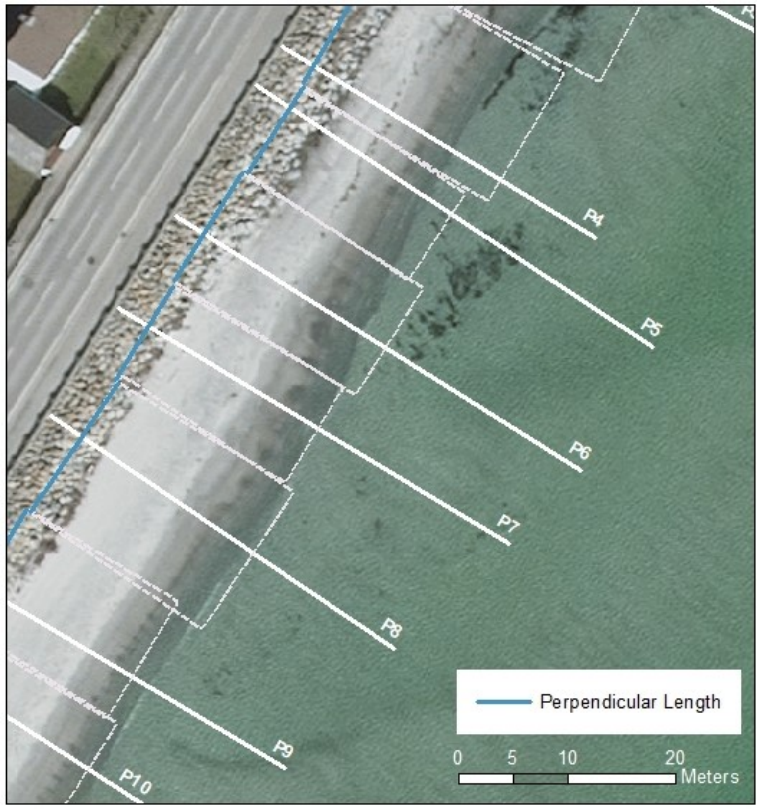

Figure 5.9: Close up view of a number of profiles that each represent one specific section of the coastal stretch, the size is dependent on the perpendicular length.

The perpendicular distance is then multiplied by the volume of sediment present in the corresponding profile. The difference between the years 2020 and 2018 was obtained to be -4330 m^3, which corresponds to a reasonable significant loss of material. By dividing this result by the time, in years, between the two separate profile surveys, i.e. 4 December 2018 and 3 March 2020, respectively, a rate is obtained. The result is -3464 m^3/yr. However, the method used does not permit any conclusions on whether the lost material has been transported in the longshore or cross-shore direction to be made. The profile survey data only represent the dry beach profile, hence the lost material can have deposited further seaward but still within the cross-shore profile and is thereby not lost from the system. Should

the material instead have been transported via longshore drift, it is lost from the system entirely.

The amount of material lost in the entire coastal section can be estimated based on losses observed in the dry part of the nourished area, and depending on the depth of closure. The total volume change, $\mathrm{d}V_{\mathrm{total}}$ is:

$$\mathrm{d}V_{\mathrm{total}} = \mathrm{d}V_{\mathrm{b}} + \mathrm{d}V_{\mathrm{h}} \tag{5.1}$$

where $\mathrm{d}V_{\mathrm{b}}$ correspond to the volume change in the dry part of the coast, i.e. change of the berm, and $\mathrm{d}V_{\mathrm{h}}$ is the volume change for the section located under water.

The active profile height, D_a, corresponds to the water level at the depth of closure (D_c) plus the height of the berm above the mean water level (B_c), according to:

$$D_a = D_c + B_c \tag{5.2}$$

It follows that the expression for the total volume change in the profile, $\mathrm{d}V_{\mathrm{total}}$, may be derived to:

$$\mathrm{d}V_{\mathrm{total}} = \mathrm{d}V_{\mathrm{b}} \cdot \frac{1 + D_c}{B_c} \tag{5.3}$$

Hence, a berm height above the mean water level of $B_c = 1.5$ m and a water depth at the depth of closure of $D_c = 4$ m yield a total volume change of $\mathrm{d}V_{\mathrm{total}} = 3.33 \cdot \mathrm{d}V_{\mathrm{b}}$. This yields a rough estimate of -14,420 m^3 of material lost between the two studied events. The procedure has been derived based on a 'Volumetric Rule of Thumb' presented by Kraus et al. (1998). The estimated loss corresponds to approximately 23% of the total volume of the initial nourishment, i.e. 62,000 m^3. This reflects quite a drastic loss of material given that the material would have been lost during the period of solely 16 months that the nourishment has been in place. To put the numbers in perspective, the estimated volumes of maintenance nourishment are 15,000 - 20,000 m^3 every fifth year, which corresponds to 24-32% of the volume used for the initial nourishment. This is roughly the same loss obtained in the analysis but at a much shorter time period. However, it should be noted that the applied procedure to estimate the total volume corresponds to an assumption which implies that all material lost in the profile has been lost through longshore transport. This is not completely accurate as there is a likely chance that the material has been transported cross-shore and deposited in the nearshore part of the profile. Although, the result provide an estimate of the maximum possible magnitude of the volume of lost material. In order to get a proper view of the situation it is important to study the amount of nourished material that may be present in the cross-shore profile. Profile surveys that extend all the way to the depth of closure, like the one conducted by boat of 3 March 2020, can be more appropriate to study to map the changes in the system more accurately.

6 Shoreline Evolution Analysis

The shoreline evolution was studied from available orthophotos, provided by The Danish Map Supply (Agency for Data Supply and Efficiency, n.d.) and analysed using ArcGIS. The ArcGIS extension software Digital Shoreline Analysis System (DSAS) version 5.0 developed by the United States Geological Survey (USGS), was used as an analysis tool to calculate the rates of shoreline change (Himmelstoss et al., 2018). The aim is to study the erosion rates and study the evolution of the shoreline over time. The shoreline position for a number of years was digitized from the orhtophotos and then analysed using DSAS to obtain rates of change.

DSAS provides a tool to calculate the rate of change between different years, based on shoreline position. Rates are calculated along perpendicular transects placed between the shoreline and a boundary (baseline), placed either offshore, onshore or midshore. For the purpose of this project, the quantity used to estimate the erosion rate with DSAS is the End Point Rate (EPR) [m/yr]. The EPR is defined as the Net Shoreline Movement (NSM), which is the distance [m] between the oldest and most recent shoreline positions, divided by the time between the oldest and most recent shorelines [years]. (Himmelstoss et al., 2018).

$$\text{EPR} = \frac{\text{NSM}}{\text{time between oldest and most recent shoreline}} \tag{6.1}$$

The seaward edge of the vegetation line typically provides a reliable measure that can be used as an indication of morphological change. It is stable on a longer time scale however, the position responds to impact with significant time lag (Boak & Turner, 2005). The vegetation line is a good indicator of morphological changes, provided that there is vegetation present. For this study, in the absence of coastal vegetation another indicator of morphological change had to be applied. The definition of the shoreline adopted in the study is instead the instantaneous water line, which is defined as the boundary between land and water. In orthophotos it is detected as a slight shade difference (light to dark) in color or in grey (Boak & Turner, 2005). Compared to the vegetation line, the water line is an indicator that presents a much quicker response to impact. Studying the water line hence provides an instantaneous view of the situation.

Prior to 2002 there were groynes placed along the beach, and hence the shoreline evolution analysis had to be restricted to the period after 2002, to get a more accurate view that resembles the current situation. Furthermore, the analysis has been divided into years before the nourishment was carried out and years after the nourishment was established. Table 6.1 presents details of the orthophotos used in the study. The orthophotos were obtained from The Danish Map Supply as WMS-maps available for download (Agency for Data Supply and Efficiency, n.d.) to be applied directly in ArcGIS. Details of date and time when the photos

had been generated were supplied by the Agency for Data Supply and Efficiency[3]. However, it was only possible to get the information from earliest 2012 which is why the study was further limited to a number of relatively recent years. Knowing the date that the orthophoto was generated is important for the analysis as it is required to compute the rates of change.

Table 6.1: Aerial photos used in DSAS analysis, (Agency for Data Supply and Efficiency, n.d.)

Year	Date[3]	Resolution (cm)	Name in Web service list
2013	2-May	10	geosjaelland_2013_10cm
2014	11-Mar	10	geosjaelland_2014_10cm
2015	10-Apr	12.5	geodanmark_2015_12_5cm
2017	6-Apr	12.5	geodanmark_2017_12_5cm
2019	15-Apr	12.5	Ortofoto forår 2019

6.1 Years Before the Initial Nourishment (2013-2017)

Between the years 2013-2017, four separate orthophotos are studied and shorelines digitized. The analysis is structured to study the EPR for one year at the time, between 2013-2015, two years between 2015-2017, and finally the entire period of four years between 2013-2017. The instantaneous water line is adopted as the definition of the shoreline. The area is confined to include the stretch of coastline between the harbour and the the outlet of Faxe Creek, and roughly 360 meters downdrift the creek outlet. Resulting in a total longshore distance of approximately 1000 meters. The DSAS analysis commenced by assigning an offshore boundary and then placing transects every five meters along the shoreline and rates of change are calculated along these transects. Maps showing the studied coastal stretch along with the results of the computed EPR is shown in Figures 6.2a-d. Positive rates (accretion) are indicated by blue shades while red shades indicate negative rates (erosion). Figures 6.3a-d present a graphic display of the results of EPR the different years, where EPR is plotted against longshore distance from the harbour.

As previously mentioned, performing shoreline evolution analysis and adopting the instantaneous water line as the definition of the shoreline provides a more instantaneous view of the situation. The analysis is sensitive to changes in the water line positioning caused by immediate conditions of waves and water level. The water line position is more variable compared to the vegetation line and does not reflect long term morphological changes as accurately. The position of the water line may occasionally rather display a reflection of the conditions leading up to the event when the orthophoto was generated. The conditions of wave height and direction along with water level have been studied in the time before and between the orthophotos used in the analysis. Figure 6.1 presents an example of the studied plots for the summer months of 2015, remaining periods are presented

[3]Eva Rosová, Agency for Data Supply and Efficiency, email contact 17 March 2020.

in Appendix. The conditions have been studied for winter and summer periods respectively, corresponding to October-March and April-September. The left plot in Figure 6.1 shows a plot of significant wave height (blue) and water level (orange) during the summer of 2015. Water level data is given in the reference system "Danish Vertical Reference 1990" (DVR90) (Danish Meteorological Institute, n.d.). The right plot in Figure 6.1 presents a wave rose for the corresponding period, to display the height and direction of the incoming waves. This material is considered in order to try and explain certain potential reasons for the morphological changes, causing response in the shoreline position.

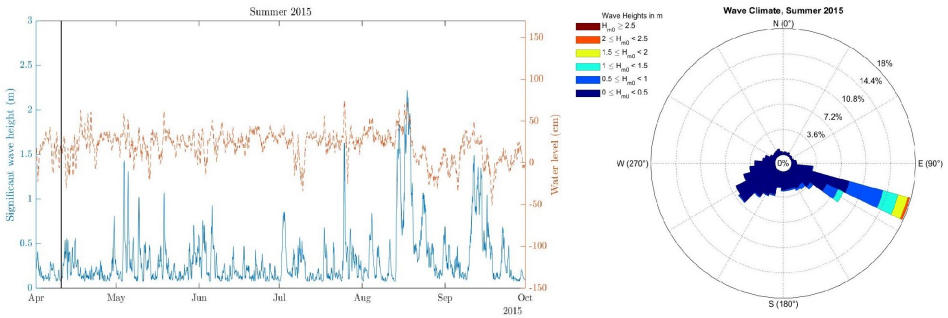

Figure 6.1: Wave and water level conditions for the period April-September 2015. The black vertical line marks event of generated orthophoto (10 April 2015).

Figures 6.2a and 6.3a present the results of EPR for the period May 2013 to March 2014. The majority of the transects located south of the creek outlet display negative EPR, indicating that the erosion is quite pronounced in this area. Positive rates are obtained for the transects in close proximity to the harbour and the creek outlet, respectively. Studying the conditions for this period showed that there was a significant storm in January 2014 with recorded wave heights greater than 2.5 meters. This event could have caused permanent or momentary changes in the beach morphology. Storm events are characterized by significant transport in the cross-shore direction, with eroded material from the berm depositing in the nearshore. The 2014 orthophoto was generated on 11 March and it is likely that the beach would have recovered from the storm impact. Sediment transport in the longshore direction, however, would cause permanent loss of material in the area which is potentially the case in the area south of the creek outlet.

Figure 6.2b presents the result of the EPR between March 2014 and April 2015. The result shows that the EPR is predominantly negative along the beach as well as the majority of the transects in the area south of the creek outlet. At a distance approximately 500 meters from the harbour, the EPR is as much as -5 m/yr. Studying the corresponding conditions during this period, show that conditions in 2014 were quite rough with H_{m0} greater than 1.5 meters recorded at a number of occasions. Towards the end of March 2015, i.e. recently before the orthophoto

was generated, there was an event with wave heights of approximately 2 meters and simultaneously a recorded water level of +70 cm. This can potentially have caused some of the change detected in the analysis, as the beach would not have had significant time to recover from the storm impact.

Figures 6.2c and 6.3c show the result of the period April 2015 to April 2017. The result in Figure 6.2c shows that the EPR is positive along transects located in close proximity to the harbour. The erosion (negative EPR) is more pronounced further away from the harbour, towards the groyne and beyond. However, a large portion of the transects showed limited change. Both orthophotos from 2015 and 2017 showed that for parts of the coastline, the revetment was exposed and no material was present in front of the structure, hence there was no change in shoreline position. This explains the limited change in the area approximately 160-500 meters from the harbour. Additionally, studying the conditions for the period, it is possible to conclude that the general wave climate was calmer than usual and that the number of significant storms were reduced. This could also be a possible explanation to the relatively reduced results of EPR that are obtained for this period. However, it is important to note that the result corresponds to a longer time period. The analysis between 2015-2017 consists of two years compared to the other periods which only consist of approximately one year each. When using only one year between the studied shoreline positions, the EPR will correspond to the NSM according to the relation in Eq. 6.1. While for the longer time period for the analysis 2015-2017 the corresponding NSM will be twice the magnitude to the EPR.

Figures 6.2d and 6.3d correspond to the result of the whole studied period, i.e. 2013-2017. The analysis provide the result of the EPR between the shoreline positions in 2013 and 2017. The result shows that the computed EPR is predominantly negative along a vast majority of the transects. The EPR becomes increasingly more negative with increasing distance from the harbour. Positive rates are obtained for the transects located in close proximity to the harbour and the transects located furthest downdrift. This result displays that even when a longer time period is considered, predominantly negative EPR is computed along the majority of the transects, suggesting that the coastal stretch is subject to erosion.

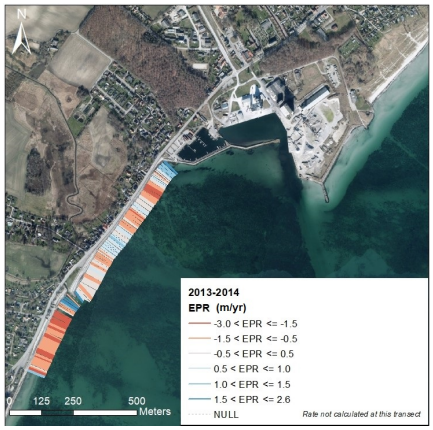

(a) 2013-2014.

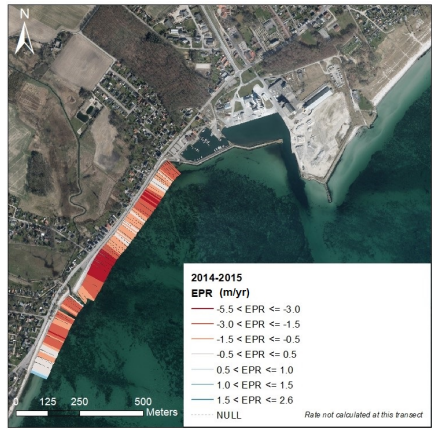

(b) 2014-2015.

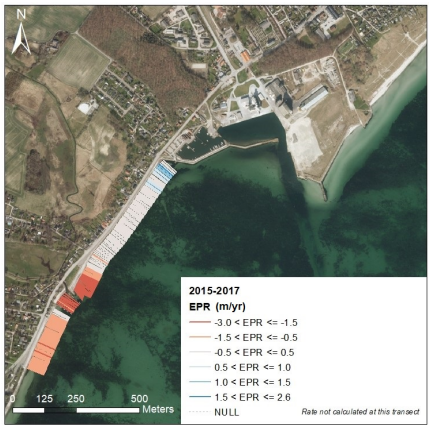

(c) 2015-2017.

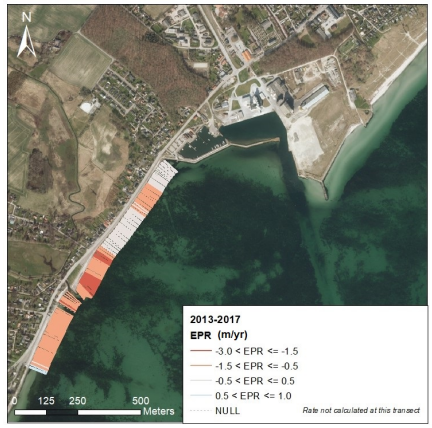

(d) 2013-2017.

Figure 6.2: End Point Rate (m/yr) in the years before the nourishment was carried out.

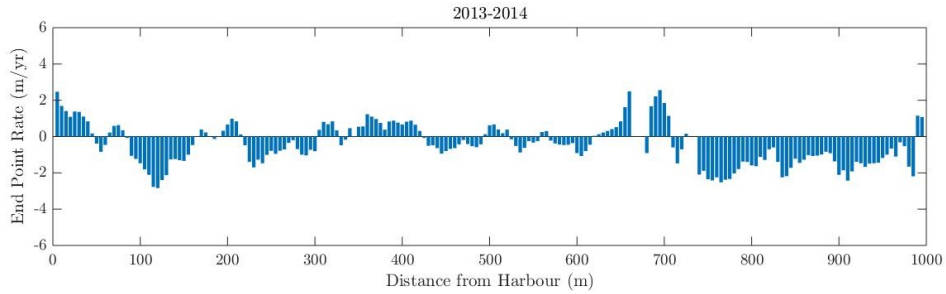

(a) 2013-2014.

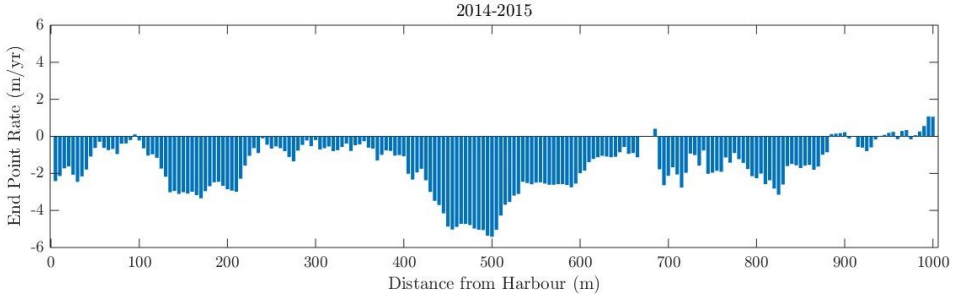

(b) 2014-2015.

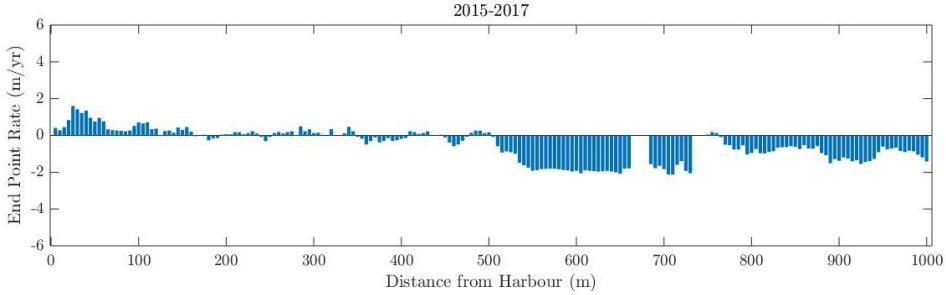

(c) 2015-2017.

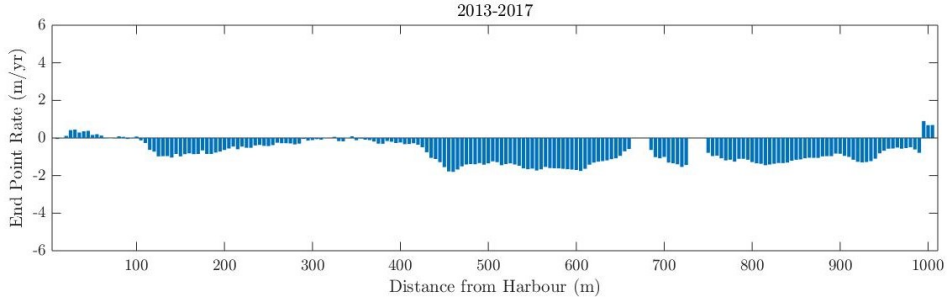

(d) 2013-2017.

Figure 6.3: Graphic presentation of End Point Rate (m/yr) year by year.

In three of the four studied periods (all except 2014-2015), the transects in close proximity to the harbour display positive rates of EPR while the overall trend is erosion for the studied coastal stretch. This can potentially be an indication that the harbour has a sheltering effect in this area, and consequently reducing the wave impact. The appearance of the corresponding graphic presentation of the results in Figure 6.3 is typical for a phenomenon known as *downdrift erosion*. Downdrift erosion is the erosion that occurs on the lee side of a natural or man-made littoral drift barrier (Bruun, 1995), for example a groyne or harbour construction in the case of this study. Downdrift erosion is characterized by that the area adjacent to a structure (on the lee side dependent on the direction of the littoral drift) accumulates sediment while the area further away from the structure erodes. On the updrift side of the structure there is accretion of material (Bruun, 1995).

Alternative Approach to Estimate Shoreline Position

There are some uncertainties related to the method of performing shoreline evolution analysis. Due to the absence of coastal vegetation at the study site, the analysis had to be restricted to solely consist of analysis of the instantaneous water line. Hence, the main uncertainties and potential sources of error are related to identifying the water line position accurately. For example in some years, the presence of large amounts of seaweed located especially in the part of the beach closest to the harbour, made it difficult to identify the actual position of the water line, which therefore had to be carefully estimated. Digitizing the shorelines takes patience and experience.

Details of date and time when the orthophotos were generated were provided by the Agency for Data Supply and Efficiency. The information made it possible to identify the exact water level at the specific occasions when the orthophotos were generated. Thereby, a second analysis was carried out when the water level was accounted for. Table 6.2 presents the recorded water level for the specific occasions when the orthophotos were generated. The data shows that the water level is quite even between the years with an average of +20 cm. However, in the years 2014 and 2017 the water level deviates from this average, in 2014 the water level was lower and in 2017 the water level was higher. Water level data is given in the reference system DVR90.

Table 6.2: Water level data.

Year	**Date and time**	**Water Level (cm)**
2013	2-May 08:30	+15.5
2014	11-Mar 11:30	+8.5
2015	10-Apr 09:30	+22
2017	6-Apr 11:30	+42
2019	15-Apr 13:00	+17

The water level is accounted for by calculating a cross-shore distance by dividing the water level with an assumed foreshore slope. As a result, in the new analysis the shoreline is set to be defined at +0 cm. Figure 6.4 shows a schematic image of the theory behind the correction. The distance dy is equal to the water level (WL), and the distance dx is the corrected distance in the cross-shore direction, k is the foreshore slope.

Figure 6.4: Schematic image showing the slope geometry.

Based on the geometry presented in Figure 6.4, the correction is calculated according to the relationship given in Eq. 6.2.

$$k = \frac{\mathrm{d}y}{\mathrm{d}x} \rightarrow \mathrm{d}x = \frac{\mathrm{d}y}{k} \tag{6.2}$$

The foreshore slope is not known and has to be assumed. A typical foreshore slope of $k_{\text{foreshore}} = 0.15$ is applied, which is assumed to represent a generic foreshore slope. The slope of the structure is known to be $k_{\text{revetment}} = 0.67$ (1:1.5) (COWI, 2013). In the cases when the water level is all the way up towards the rock revetment, the slope of the structure is used. The analysis originated from the initially digitized shoreline which is simply corrected with the computed cross-shore distance, dx. The analysis of EPR is conducted as previously described. Figures 6.5a-d present the difference in computed EPR between the original analysis (blue line) and when the water level was accounted for (orange bars). Figure 6.5a presents results where the initial positive computed EPR generally is higher than the corrected result while the initial negative computed EPR generally is lower than the result of the corrected analysis. The analysis of EPR for the period 2013-2014 corresponds to a situation when the water level is higher in the most recent year of the analysis, see Table 6.2 for water level data. This can potentially suggest that when the water level is higher in the earliest year of the analysis, the accretion is overestimated while the erosion is underestimated. The remaining periods (Figures 6.5b, 6.5c and 6.5d) present results where the initial positive EPR generally is lower than the corrected result while the initial negative computed EPR generally is higher than the corrected result. Consulting Table 6.2 to compare water level data, this can potentially suggest that when the water level is higher in the earliest year of the analysis, accretion is underestimated while erosion is overestimated.

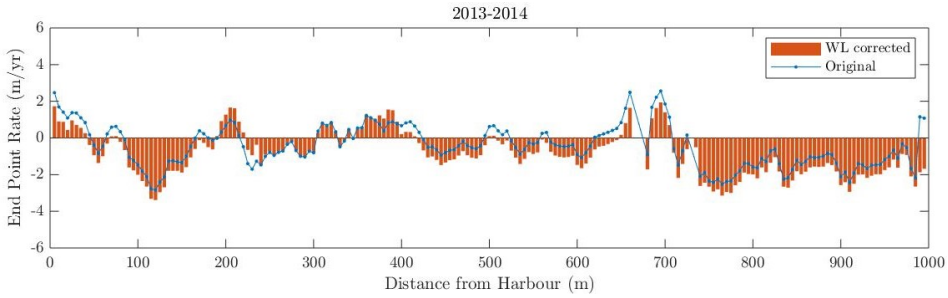

(a) 2013-2014.

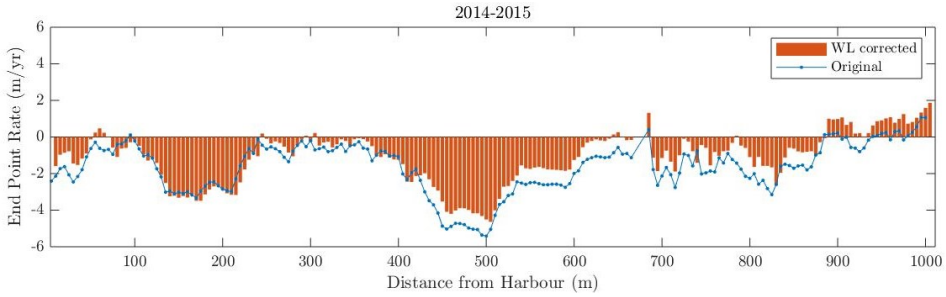

(b) 2014-2015.

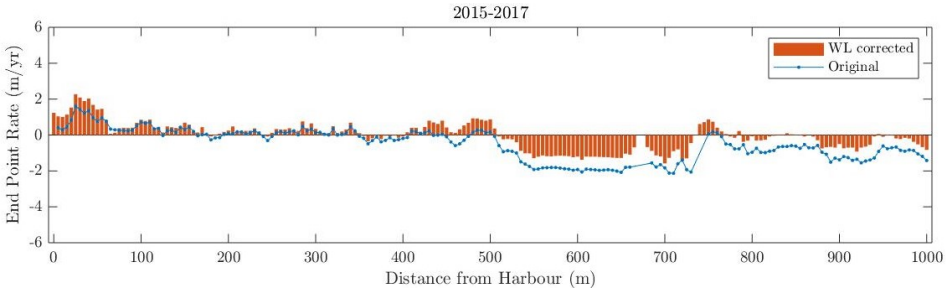

(c) 2015-2017.

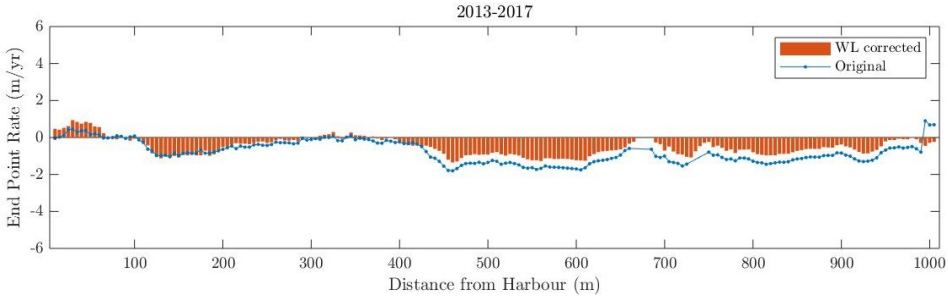

(d) 2013-2017.

Figure 6.5: Graphic presentation of End Point Rate (m/yr) year by year when the water level is accounted for.

The results in Figures 6.5a-d show a slight difference in computed EPR between the two conducted analyses, however, the magnitude is generally not significant. The alternative approach, when the water level is accounted for was possible to complete since the water level at each occasion of the orthophotos was known. However, details of foreshore slope are required which had to be assumed and this is a limitation of the method. The main challenge of the procedure is to accurately estimate the value of the foreshore slope k. The foreshore slope used for the correction is expected to have significant impact on the corrected distance, due to geometry. A gentler slope gives a larger corrected distance while a steeper slope (for example at the slope of the structure) has limited effect. The corrected result is calculated by assuming a foreshore slope and applying the same slope to all the studied years. This can generate an uncertainty of the method as the foreshore slope can vary significantly along the longshore distance.

6.2 Years After the Initial Nourishment (2019-2020)

The shoreline analysis for the period April 2019 to March 2020 represent a time period after the initial nourishment was carried out. The analysis consists of digitized shorelines from 15 April 2019 and 3 March 2020. The 2020 shoreline was derived from profile data collected on the day of the field measurements, that provided details of the elevation in the cross-shore and longshore directions. The 2020 shoreline could hence be generated by simply considering the points at +0 m elevation. This cause the definition of the shoreline to be at +0 m. The 2019 shoreline was digitized from an orthophoto available as WMS-download through the Danish Map Supply (Agency for Data Supply and Efficiency, n.d.). In order to assure the same definition of the shoreline the 2019 shoreline was corrected with respect to the water level according to the methodology previously described. The foreshore slope adopted for the correction, was carefully estimated based on profile measurements from 3 March 2020. The slope south of the creek outlet was found to be slightly steeper than in the nourished area. The slopes were approximated to be $k_{\text{south}} = 0.086$ and $k_{\text{nourishment}} = 0.07$, respectively. The obtained slopes are not as steep as the assumed foreshore slope used in the previous analysis ($k = 0.15$), as the slope was derived from real data and corresponding to a storm profile measured on 3 March 2020. A beach profile formed during storm impact typically has a flattened foreshore slope compared to the slope of a calm beach profile (Komar, 1998). The value used in the previous analysis of $k = 0.15$ is hence considered to correspond to a generic foreshore slope of a calm beach profile. The values $k_{\text{south}} = 0.086$ and $k_{\text{nourishment}} = 0.07$ were used for correcting the shoreline position based on the water level. The DSAS tool was used to compute the End Point Rate (m/yr) in the same manner as previously described. Figure 6.6 shows a map of the results of EPR along the transects, where negative rates (erosion) are displayed with red shades and positive rates are indicated by blue shades (accretion). Figure 6.7 presents the result graphically, where EPR is plotted against longshore distance from the harbour.

The results in Figures 6.6 and 6.7 show that the transects closest to the harbour (the first 100 meters) experience accretion. This is potentially due to the area being sheltered by the harbour, causing waves to be smaller in this area. The subsequent section of the coastline, i.e. the section located at a distance 200-600 meters from the harbour, shows that the erosion is quite extensive. Similarly to the result of EPR for a number of the studied periods prior to the initial nourishment action, the appearance of the graph in Figure 6.7 is typical for the phenomenon known as downdrift erosion. For the transects located just before the groyne, the EPR is positive. This is most likely due to that the groyne accumulates sediment. Furthermore, the results show that the area south of the outlet of Faxe Creek mainly experience positive rates of EPR, and the computed erosion is relatively low. It is possible that material from the nourished area has bypassed the groyne and deposited in the area south of the creek outlet.

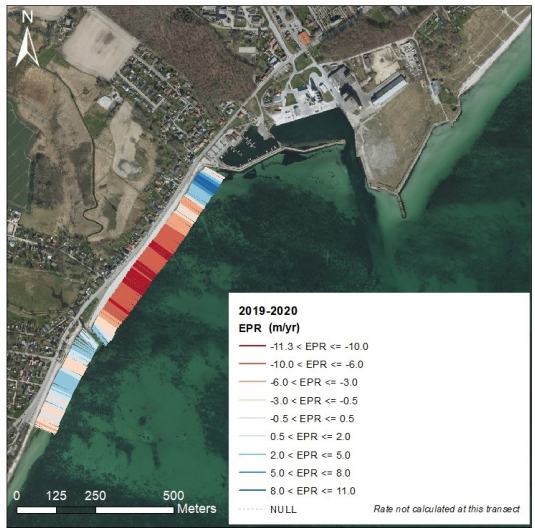

Figure 6.6: End Point Rate (m/yr) between 2019-2020.

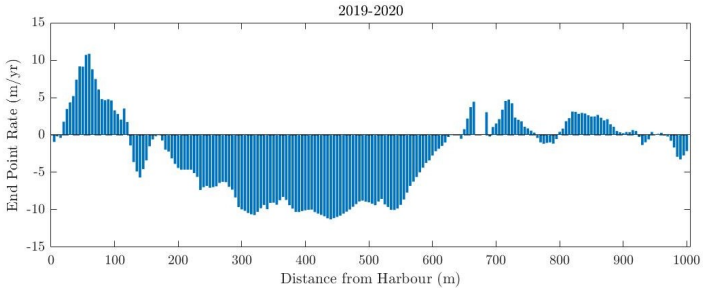

Figure 6.7: End Point Rate (m/yr) between 2019-2020.

The results of EPR obtained from DSAS analysis for the years after the initial nourishment compared to the years before, show significantly more negative results, i.e. more pronounced erosion. The explanation to this can potentially be that the nourishment provided material to the system which was not available previously. In the period before the nourishment was in place, the abundance of material in the profile was limited. For example, during the later years 2015-2017 the revetment structure was fully exposed and no material located in front of it, hence yielded low values of EPR as the shoreline was stable and did not move. Additionally, the difference between the results was possibly further amplified by the fact that the profile measured during the field study on 3 March 2020, was a storm profile.

The photos in Figures 6.8 and 6.9, provided by the Municipality of Faxe, show the difference in the appearance of the beach in January and April 2020. The photos display great differences in the beach morphology between the two occasions, which can indicate that there is a strong dynamic behaviour of the beach. The photos from 13 January 2020 display a clear storm profile with signs of recent erosion. While the photos from 8 April 2020 show a beach profile typically generated at calm conditions. The images suggest that the seasonal variation of the beach profile in the area is quite significant. During storm conditions, eroded material is deposited offshore, to later be transported back to the beach plane during calm conditions and the beach recovers. Data shows that the water level during the day on 13 January 2020 was roughly +40 cm which is higher than the average. The water level on 8 April 2020 however, is unknown. It should be noted that a difference in water level potentially can contribute to the some of the recorded difference in appearance between the two occasions. If the water level on 8 April was significantly lower compared to 13 January the increase of the beach width would appear greater.

(a) 13 January 2020.

(b) 8 April 2020.

Figure 6.8: Figures showing the beach plane, with the harbour in the background (north view). Photo: Poul Jensen, Municipality of Faxe, 2020.

(a) 13 January 2020.

(b) 8 April 2020.

Figure 6.9: Figures showing the beach plane in the direction of the groyne (south view). Photo: Poul Jensen, Municipality of Faxe, 2020.

The result in Figure 6.7 presents significant negative values of EPR obtained for the period after the nourishment was established, suggesting that large amounts of material is lost from the beach profile. However, that does not have to equal that the material is lost from the system entirely. The photos in Figures 6.8 and 6.9 show that the beach has gone from having a dominant storm profile to a profile characteristic for calm conditions. This difference in appearance between two relatively recent events, can indicate that some material had been transported and deposited in the cross-shore profile. Which since the field investigation on 3 March 2020 partly has migrated onshore during periods of calmer conditions, and the beach has recovered resulting in a wider beach place. Although the seasonal variation is quite noticeable the result of the shoreline evolution in the years before the nourishment was carried out, generally show an erosive long-term trend. It is thereby possible that some material has been transported longshore and is hence lost from the system. The results of EPR for the period after the initial nourishment was carried out (presented in Figures 6.6 and 6.7) should however be evaluated with caution, as 2020 corresponds to a storm profile. The result clearly showcases the sensitivities related to adopting the instantaneous water line as the definition of the shoreline. It is important to emphasise that the orthophoto only presents one momentary image to represent an entire period.

7 Numerical Modelling

7.1 Modelling of Longshore Sediment Transport Rate

To calculate the rate of potential longshore sediment transport, a FORTRAN program that applies the CERC-formula is used. The CERC-formula (U.S. Army Crops of Engineers, 1984) is presented in Eq. 7.1,

$$Q_{\mathrm{ls}} = \frac{K}{16(s-1)(1-P)} H_{\mathrm{sb}}^2 C_{\mathrm{gb}} \sin(2\alpha_{\mathrm{b}}) \tag{7.1}$$

where $Q_{1\mathrm{s}}$ is the rate of potential longshore sediment transport, s is the relative sediment density, P is the sediment porosity of typically 40% and K is an empirical coefficient. The breaking wave conditions applied in the equation include H_{sb} which is the significant wave height at breaking, C_{gb} is the wave group celerity at breaking and α_{b} is the incident wave angle at breaking.

The breaking wave conditions H_{sb} and α_{b}, are computed based on the conservation of wave energy flux and Snell's law, equations 7.2 and 7.3, respectively (U.S. Army Crops of Engineers, 1984). The model hence assumes straight and parallel bottom contours. Equations 7.2 and 7.3 are solved numerically to obtain the conditions in the breaking point. The breaking criteria $H_{sb} = \gamma h_b$ is hence applied, where h_b is the breaking depth and γ is equal to 0.78.

$$H_{\mathrm{s0}}^2 C_{\mathrm{g0}} \cos\alpha_0 = H_{\mathrm{s\ b}}^2 C_{\mathrm{g\ b}} \cos\alpha_{\mathrm{b}} \tag{7.2}$$

$$\frac{\sin\alpha_0}{C_0} = \frac{\sin\alpha_{\mathrm{b}}}{C_{\mathrm{b}}} \tag{7.3}$$

where H_{s0}, C_{g0}, C_0 and α_0 are the significant wave height, group wave celerity, phase velocity and wave angel at the offshore point. While, H_{sb}, C_{gb}, C_{b} and α_{b} are the wave parameters at the breaker line.

The offshore wave conditions are required as model input, parameters include significant wave height H_{m0}, peak period T_p and wave direction θ. Furthermore, the shoreline orientation has to be assigned when the model is run. The model computes the potential longshore sediment transport rate, which is presented in the unit of m^3/yr.

The sediment transport is defined as positive in the southward direction and negative in the northward direction. Running the model yield a result of the average annual potential net longshore transport rate of 73,000 m^3/yr. The model used in the project was calibrated with parameters corresponding to a previous study conducted at Falsterbo in southern Sweden (Wang, 2019). Since the model performance may not be completely accurate there are a lot of uncertainties of the

generated results. Due to this, normalized transport is instead studied. For this application the calibration is assumed to be sufficient to apply for the purpose of this study. Normalized results provides a display of the magnitude of the transport rate during the simulated period. Annual and monthly rates have been studied and the values were normalized with the annual and monthly average net transport rates, respectively.

The result presented in Figures 7.1 and 7.2 confirms that the net transport is southward directed. Figure 7.1 shows the normalized annual net longshore transport rate between 2006-2019. During the simulated period, the potential net longshore sediment transport rate varies between roughly half to twice the average net rate. A significant peak is detected in year 2014. This recorded peak in annual potential longshore sediment transport provide a potential explanation to the result of the shoreline evolution analysis. The largest negative EPR computed in the period before the initial nourishment was obtained in the period March 2014 to April 2015, which hence corresponds well with the peak in Figure 7.1.

Figure 7.2 presents the result of the monthly variation of net longshore transport rate, where the values have been normalized with the monthly average potential net transport rate obtained for the whole simulated period. The result provides a view of how the transport typically varies throughout the year. The result shows that the largest potential net longshore transport rate is obtained in January-March. The months with the lowest potential net rate are June-July. The appearance of the graph displaying the monthly variation of longshore transport rate correspond well with the result of monthly average significant wave height. During the months with generally calmer conditions, i.e. April-September, the computed rate is typically lower. While during the months with rougher conditions, i.e. October-March, the potential net sediment transport rate is generally higher. The result of net transport rate also reflects the wave climate during the simulated period, as the model is based on offshore wave climate data as input.

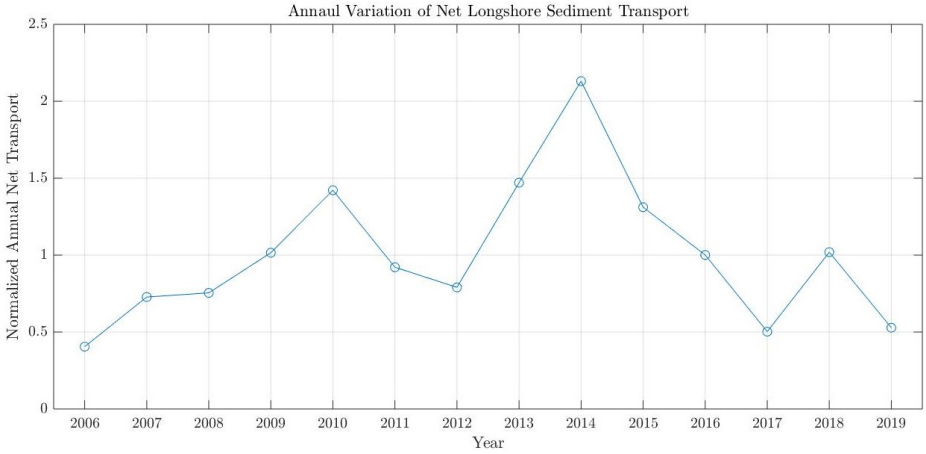

Figure 7.1: Annual variation of potential net longshore sediment transport rate, note that the result is normalized with the annual net transport rate hence unit less.

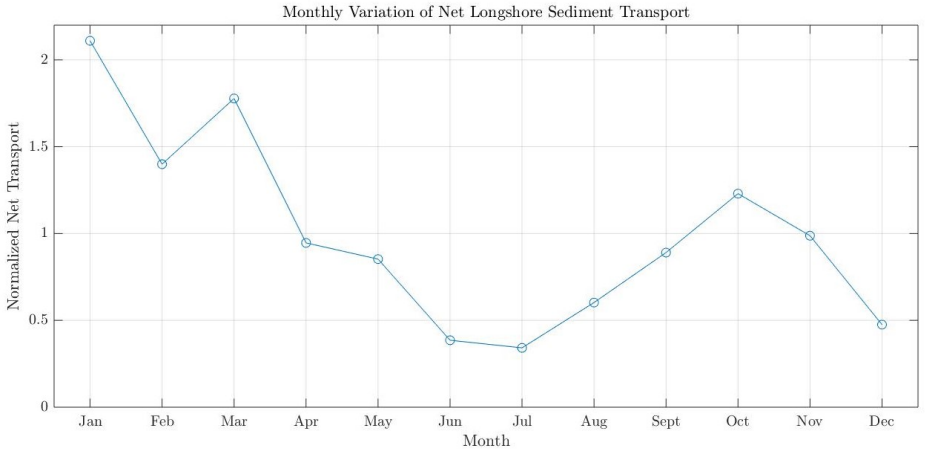

Figure 7.2: Monthly variation of potential net longshore sediment transport rate, note that the result is normalized with the monthly average net transport rate hence unit less.

The initial nourishment was carried out at the end of 2018, Figure 7.1 shows that the net lonsgshore transport rate in the subsequent year, 2019, was lower than average, with a normalized net transport rate of 0.5. The result presents the potential transport rate and hence it would suggest that during the first period that the nourishment was in place, the conditions were reasonably mild and potentially the added material was not removed by longshore transport to an abnormal extent.

7.2 Nearshore Wave Transformation

The nearshore wave transformation model EBED, produced by Mase (2001) and later modified by Nam et al. (2009) was used to study the wave field around the harbour and the nourished area. The model is a multi-directional random wave transformation model, based on the energy balance equation and includes energy dissipation and diffraction terms. The physics of the model are briefly explained in Appendix. The model requires bathymetry and offshore wave conditions as input, as well as some operational parameters such as grid size and spectral resolution. To conduct the simulations, a grid with a cell size of 5x5 meters was used to run the model. Figure 7.3 shows the orientation of the grid and the highlighted line marks the input boundary which corresponds to the y-axis.

The bathymetry required for the simulations was derived from a map with contour lines presented by Ramboll (2016b) in combination with the profile measurements collected on 3 March 2020 to get a more detailed description closer to the shore. The nearshore wave transformation model computes three wave parameters in each cell of the grid; significant wave height (H_s), significant wave period (T_s) and mean wave direction ($\bar{\theta}$).

Figure 7.3: Orientation of the bathymetric grid applied in EBED, the highlighted line marks the input boundary.

A wave with conditions $H_{m0} = 1.07$ m and $T_p = 5.66$ s was simulated with altering incoming wave direction θ. The wave corresponds to a typical medium sized wave in January, however waves around one meter in height are recorded in all the months of the year. Four different incoming wave directions (θ) were simulated, i.e. 80°, 110°, 140° and 180°, see Figure 7.4. The input boundary limits the model to only

be able to simulate waves within a range 180°. As the incoming wave directions become more parallel to the input boundary the model performance decreases. The four simulated incoming wave directions were hence applied to represent a diverse spread. The result of the model simulations were used to plot the wave field around the harbour and the nourished area, the results are presented in Figure 7.5. The result shows that at $\theta = 80°$ (Fig. 7.5a) it is possible to detect that the area adjacent to the harbour is sheltered, as the computed wave height in this area is slightly smaller, indicated by light blue colors. As the incoming simulated wave angle increases, so does the computed wave height, and the sheltering effect of the harbour is reduced as waves approach more perpendicular to the shoreline. The largest computed wave heights are obtained at $\theta = 110°$ and 140°. The orange areas visible in Figures 7.5b and c correspond to a significant wave height greater than the height of the simulated wave ($H_s = 1.07$m) and is an effect of shoaling. The area becomes progressively more shallow as the shore is approached, causing waves to break. The wave height decreases which is indicated by the shade transitioning from yellow to blue.

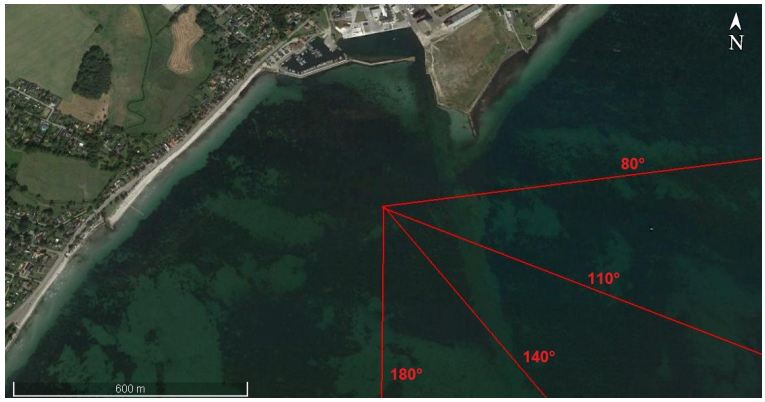

Figure 7.4: Directions of the four separate simulations. (Graphics: Google Earth Pro, 2020).

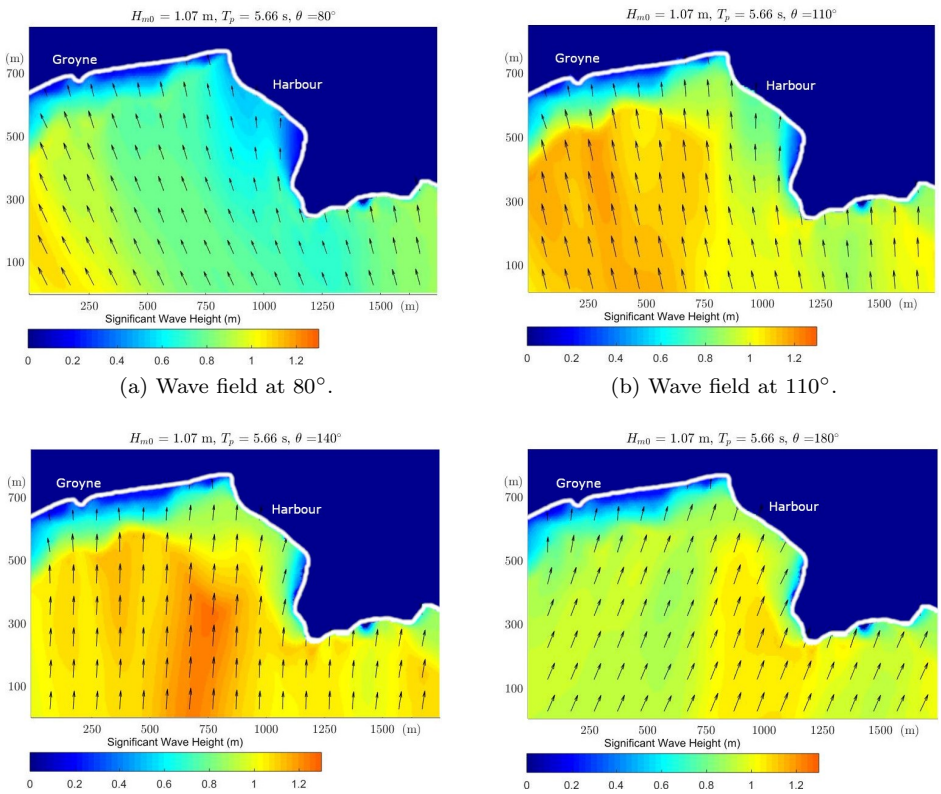

(a) Wave field at 80°.

(b) Wave field at 110°.

(c) Wave field at 140°.

(d) Wave field at 180°.

Figure 7.5: Results if EBED simulations.

The wave height and angle are more closely studied in 11 specific points located between the harbour and past the groyne. The points are placed on the -1.5 meter contour and spaced 50 meters apart, see Figure 7.6. The computed wave angle in relation to the shoreline orientation is determined and the result enables for estimation of the direction of longshore sediment transport in the specific points. Four separate simulations were performed, in the same different incoming wave angles as previously and the result is presented in Figures 7.7a-d. The result shows that at an incoming angle of $\theta = 80°$ and 110°, the longshore sediment transport is directed southward. This indicated that the longshore transport is continuously southward directed within this range. At $\theta = 140°$ the transport is directed southward in about half of the points and northward in the rest. This would indicate that at $\theta = 140°$ the direction of the longshore transport changes and becomes progressively more dominant in the northward direction. The result of $\theta = 180°$ displays a situation where the longshore transport is directed northward in all the studied locations.

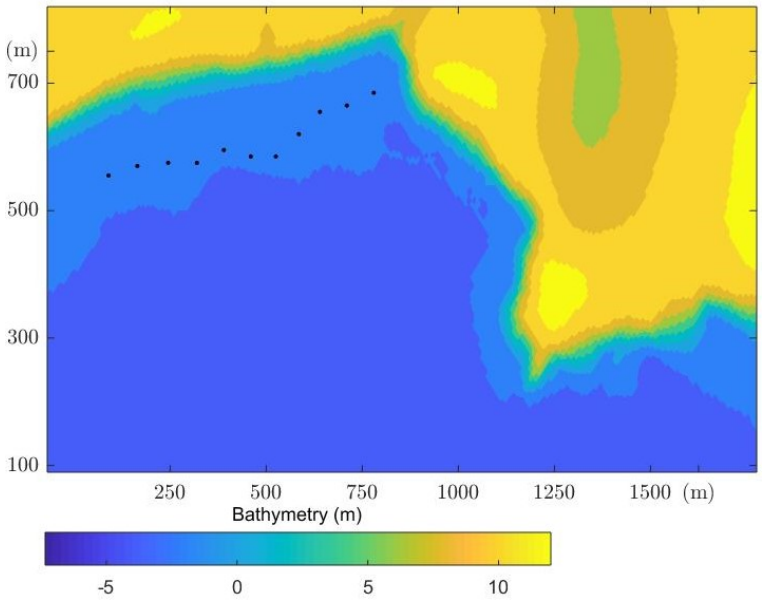

Figure 7.6: Bathymetry and point locations.

As indicated by the wave rose presented in section 3.3 in the report and discussed in the corresponding paragraphs the largest and most frequent waves recorded are in the direction θ = 100-120°. It is in these directions where the fetch lengths are the greatest. The results of the EBED-modelling show that at these directions the longshore sediment transport is directed southward. This is in line with that the dominant net sediment transport is directed southward as the result of the longshore sediment transport modelling confirms. Dominant northward direction of longshore transport is obtained at larger values of θ. However, studies of the wave climate conditions at Faxe Ladeplads suggest that waves in directions θ = 180-270° do occur although they are less frequent than waves in directions θ = 100-120°. This is expected to have an impact of the magnitude of the northward direction of the sediment transport.

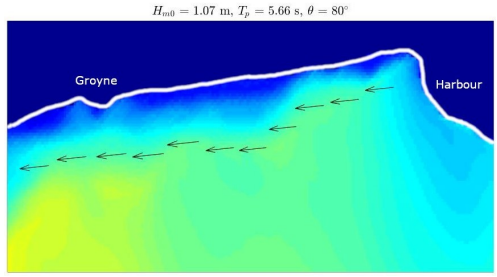

(a) 80°.

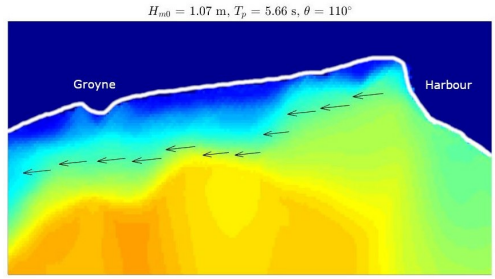

(b) 110°.

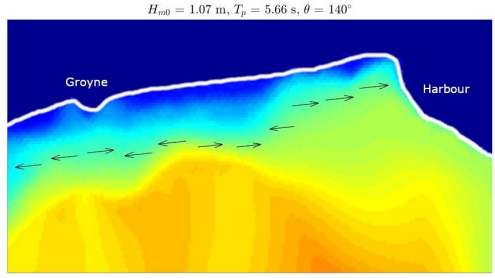

(c) 140°.

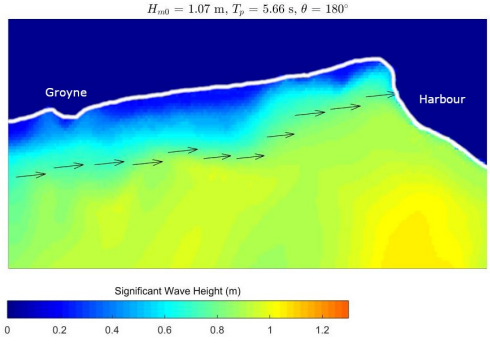

(d) 180°.

Figure 7.7: Display of direction of longshore sediment transport in the 11 different points located on bottom contour -1.5 m.

8 Discussion

8.1 Grain Size Distribution Analysis

The study of variation of median sediment grain size, based on samples collected on 3 March 2020, showed a clear trend of sediment sorting in the cross-shore direction. The results show that the largest median grain size is recorded in the swash zone followed by the reference point. The finest material in the beach plane is typically found in the aeolian deposits, while the finest material in the nearshore is at the larger water depth. These results are considered reliable as the detected distribution resembles the result presented in similar studies (Guillen and Hoekstra, 1997; Narra et al., 2015). The result of median grain size variation in the longshore direction suggests that there is limited exchange between the nourished area and the area north of the harbour. The characteristics of the samples sourced in the area down drift the nourished area indicate that there is the possibility of material from the nourishment being transported via longshore drift and deposited in this area. However, the samples in this area were scarce and the analysis is based on solely 1-2 samples per sampling point and therefore potentially not representative for an entire area.

The grain size distribution analysis provides an instantaneous view of the grain size distribution in the longshore and cross-shore directions. Weather conditions, including waves, wind and water level, impact the sediment transport and hence influence the sediment sorting in the coastal zone. For example during periods with high energy waves, median grain size is generally coarser compared to calm periods (Narra et al., 2015). The cross-shore distribution trend is not expected to differ significantly throughout the year, but rather the magnitude of the recorded d_{50}. The variation in the longshore direction may vary and is dependent on the magnitude and direction of longshore sediment transport. To better understand the transport patterns in the coastal area around Faxe Ladeplads, it can be favorable to conduct further studies of d_{50} variation during different parts of the year to represent different conditions.

8.2 Beach Morphology

The result of the volume calculations yielded an estimation of 14,420 m^3 of material that has been lost in the period between December 2018 and March 2020. The volume corresponds to 23% of the volume of the initial nourishment, which reflects quite a significant loss of material. Furthermore, the obtained result is significantly higher than the estimated volume needed for maintenance nourishment of 15,000 - 20,000 m^3 every fifth year (Ramboll, 2017). This would suggest that the estimated amount required for the maintenance nourishment according to Ramboll is not sufficient based on the results of this study. However, the result obtained in this study is based on the losses observed in the dry part of the beach profile and therefore assumes that the lost material has been transported via longshore drift. It is suggested that nourished material has deposited further out in the nearshore

profile and hence the estimated volume of lost material is overestimated. In addition, it is important to note that the most recent profile survey corresponds to a storm profile measured on 3 March 2020, which most likely magnified the losses computed in the dry beach plane.

Three of the profiles located in the middle of the area south of the creek outlet displayed an exceptional result as they reached out at a longer cross-shore distance, compared to adjacent profiles and profiles in the nourished area. This observation suggests that this area is much shallower and it is an indication of continuous build-up of sediment. It is possible that this is formed by nourished material that has bypassed the groyne. Unfortunately there are no previous surveys to compare with in order to confirm this hypothesis. However, the result of EPR for the area south of the creek outlet showed that the area typically was subject to erosion prior to the nourishment action, with the majority of transects displaying negative rates of EPR in all of the studied periods. While in the analysis corresponding to the period after the nourishment was in place, this area experienced dominating positive rates of EPR. This can be an indication that nourishment material has bypassed the groyne and deposited in the area south of the creek outlet. Hence, suggesting that nourishment material has transported via longshore transport.

The studies of EPR along the nourished area, both before and after the nourishment was in place, show that there is a general erosive trend. However, the computed EPR for the period after the nourishment shows significantly more negative results although the wave conditions generally have been milder. This may potentially be explained by the fact that the nourishment supplies material to the system that was not available previously, which magnifies the effect. The results for both the years before and after the nourishment was in place, show indications of potential lee side erosion in the area between the harbour and the downdrift groyne. This is identified as the area adjacent to the harbour experience accretion while the area further downstream of the harbour is subject to erosion. Bruun (1995) stated that bypass procedures are required to balance downdrift erosion at littoral drift barriers, such as harbours. Hence, more active and effective solutions of bypass operations should be implemented to combat lee side erosion at Faxe Ladeplads. The volumes of clean material extracted from the dredged volumes are not sufficient to meet the losses of nourished material. Instead the area located updrift of the harbour pier should be investigated to serve as the source of sediment (Nielsen, 2018). Removing material from this area may in addition potentially help to reduce the need for dredging of the navigation channel. This will supply the starved downdrift area with sediment and result in reduced rates of erosion along the nourished area and provides a solution that re-establishes the natural longshore transport (Nielsen, 2018).

8.3 Numerical Modelling

The modelling of longshore sediment transport displays how the rate of potential transport varies throughout the year. The results confirm a net longshore transport

that is predominant in the southward direction, as stated in literature (Mangor et al., 2010; Ramboll, 2017). The result of the annual variation of potential longshore sediment transport rate is a reflection of the wave climate during the simulated period. It suggests that the potential rate of longshore sediment transport for 2019, i.e. a period when the nourishment was in place, was less than average. Hence, the rates of losses of material in the nourished area has the potential to be greater than those observed in this study, in future periods.

Studies of the wave field in the area around the harbour and the nourished area show that at incoming wave angles closer to north there is a sheltering effect of the harbour. As the incoming wave angle increases so does the wave height in front of the nourished area, as waves approach more perpendicularly to the shoreline. The direction of longshore sediment transport has been estimated to be predominantly directed southward at incoming wave angles of approximately $\theta < 140°$. For waves approaching from more southerly directions, the longshore sediment transport gradually becomes directed northward. However, the wave conditions causing northward transport do not occur as frequent as the conditions generating southward longshore sediment transport.

8.4 Further Research

Through the work of this study it is recommended that continuous mapping of the cross-shore beach profiles is carried out. To benefit future studies of the morphological evolution, it is suggested that cross-shore surveys are carried out regularly and it is important that the profiles extend all the way to the depth of closure. This will enable to estimate the amount of nourished material that is present in the nearshore, and map the transport of nourished material. It is suggested that a profile survey is conducted for conditions corresponding to a calm beach profile. When compared with the results presented in this study, it will enable for better understanding of the seasonal variability of the beach and the potentially dynamic behaviour of the nourishment. Furthermore, it is suggested that the area south of the creek outlet is included for investigation as well. Studying the evolution of this area may enable for estimation of how far downdrift in the longshore direction that the nourishment material may extend and impact areas downdrift.

The objectives with the nourishment action was to reduce wave overtopping on to the adjacent road Strandvejen and to establish a beach for recreation (Ramboll, 2017). This thesis project has focused on evaluating the nourishment by studying the morphological evolution and considering the beach width. A complementary study could hence be conducted that focuses on determining the impact that the nourishment has had on reducing wave overtopping. This would serve as an additional way to evaluate the performance of the nourishment.

9 Conclusions and Recommendations

The study yielded a result showing that 23% of the volume of the initial nourishment has been lost from the nourished area, since it was carried out. Losses of this magnitude were expected in a period of five years, but the nourishment had, at the time that this project was conducted, only been in place for 16 months. The obtained result implies that the initial estimated volumes required for regular maintenance nourishment are not sufficient and have to be revised. However, the result of total volume losses in the entire profile presented in this study is based on observations of losses in the dry part of the profile where storm conditions may have amplified the result. It is hence recommended that the volume of material present in the nearshore region is accurately evaluated prior to the first planned maintenance nourishment.

The study has identified transport of nourishment material in both longshore and cross-shore directions. Results suggest that material from the nourished area bypasses the groyne and deposits in the area downdrift of the nourishment. The examined variation of median grain size in the longshore direction indicates that there is limited exchange of material between the nourished area and the area north of the harbour. While the samples collected downdrift the nourished area displayed more resemblance to the sediment characteristics of the nourished area. Furthermore, indications of significant cross-shore transport is identified in photos where the beach has recovered from previous storm impact. This suggests that there is a dynamic behaviour of the nourishment which influences the beach appearance. In addition, the study presents results that suggest that the area between the harbour and the groyne is subject to downdrift erosion as an effect of the close proximity to the harbour. The effect of downdrift erosion is concluded to have significant impact on the morphological development of the nourishment.

To combat the problems of lee side erosion it is recommended that a more proactive approach regarding a potential bypass solution of sediment is considered and further investigated. The current permit issues clean dredged material from the navigation channel to be deposited in the nourished area. However, these volumes are insufficient to cover the required amounts. Instead it should be considered to source material on the updrift side of the harbour pier, as there is accretion of sediment in this area which is estimated to be of more suitable quality. This would also correspond to artificially re-establishing the longshore transport in the natural direction of the longshore drift. The cheapest and easiest option would be to conduct this bypass operation facilitated by trucks and boats. However, installing a permanent pipe solution may be more viable and beneficial in the long-term perspective. The most expensive and advanced option would be to re-construct the harbour and to implement a new design that allows for longshore drift in the natural direction. For this, more research is required.

10 References

Aasbjerg, A. (2002). *Fakse Ladeplads - Lidt om havnenes historie*. (In Danish).

Agency for Data Supply and Efficiency. (n.d.). Kortforsyningen - Webservice liste. https://kortforsyningen.dk/indhold/webservice-liste. Accessed: 2020-02-21.

arkiv.dk. (n.d.-a). Skaderne efter stormfloden beses. Stormfloden 1904, Strandvejen, Faxe Ldp. https://arkiv.dk/vis/3944461. Accessed: 2020-02-29.

arkiv.dk. (n.d.-b). Strandvejen i Faxe Ladeplads efter storm, 1904. https://arkiv.dk/vis/262789. Accessed: 2020-02-29.

Baden, E., & Aarosiin-Hansen, J. (2017). Beach Restoration and Erosion Protection on the Inner Danish Coasts – A Case Study. *Coastal Dynamics*, (237).

Boak, E., & Turner, I. (2005). Shoreline Definition and Detection: A Review. *Journal of Coastal Research*, *21*(4), 688–703.

Bruun, P. (1995). The Development of Downdrift Erosion. *Journal of Coastal Research*, *11*(4), 1242–1257.

COWI. (2013). *Klimatilpasning - Kystbeskyttelse ved Faxe Ladeplads*. COWI, Kongens Lyngby. (In Danish).

Danish Coastal Authority. (n.d.). Coastal Protection in Denmark. https://kyst.dk/english/coastal-protection-in-denmark/. Accessed: 2020-04-25.

Danish Coastal Authority. (2016). *Kortlægning af erosion og oversvømmelse*. Danish Coastal Authority. (In Danish).

Danish Coastal Authority. (2017a). *Tilladelse til bypass efter kystbeskyttelsesloven med rent oprensningssand ved Faxe Ladeplads, Faxe Kommune*. Danish Coastal Authority. Lemvig. (In Danish).

Danish Coastal Authority. (2017b). *Tilladelse til etablering af strand ved sandfodring som kystbeskyttelse ved matr. 8bb Hylleholt By, Hylleholt, 4654 Faxe Ladeplads*. Danish Coastal Authority. Lemvig. (In Danish).

Danish Coastal Authority. (2020). Kystdirektoratets Kystatlas. http://kms.maps.arcgis.com/apps/webappviewer/index.html?id=8669133b3f4842b7a9a19fb24b08ffd5. Accessed: 2020-02-04.

Danish Meteorological Institute. (n.d.). Vandstand. https://www.dmi.dk/dmis-vejrprodukter/vandstand/. Accessed: 2020-03-19.

Danmarks Miljøportal. (2020). Danmarks Arealinformation. https://arealinformation.miljoeportal.dk/html5/index.html?viewer=distribution. Accessed: 2020-01-29.

Davidson-Arnott, R. (2010). *Introduction to Coastal Processes and Geomorphology.* Cambridge University Press.

Dean, R., & Rosati, J. (2009). Beach nourishment. In: Young, K.C. (ed.) *Handbook of Coastal and Ocean Engineering*, 843–866.

Deltares. (2016). *MorphAn 1.5.0 - Analytical tool for sandy coasts. User Manual.* Deltares.

DR. (2014). Danmarks kyst er blevet 1.436 kilometer længere. https://www.dr.dk/nyheder/indland/danmarks-kyst-er-blevet-1436-kilometer-laengere. Accessed: 2020-04-25.

Faragò, M., Rasmussen, E., Fryd, O., Rønde-Nielsen, E., & Arnbjerg-Nielsen, K. (2018). *Coastal protection technologies in a Danish context.* Vand i Byer – Innovationsnetværk for klimatilpasning, Taastrup, Denmark.

Faxe Municipality. (2019). Strandvejen nord for Faxe å. https://www.faxekommune.dk/borger/teknik-miljoe/natur/kystbeskyttelse/strandvejen-nord-faxe-aa. Accessed: 2020-02-24.

Fredsøe, J., & Deigaard, R. (1992). *Mechanics of coastal sediment transport* (Advanced Series on Ocean Engineering - Volume 3). World Scientific.

Geological Survey of Denmark and Greenland (GEUS). (2014). Den danske havbund. *Geoviden*, *2*(In Danish).

GEUS. (2020). Geological Survey of Denmark and Greenland (GEUS) - Webshop. https://frisbee.geus.dk/geuswebshop/index.xhtml/. Accessed: 2020-02-07.

Guillen, J., & Hoekstra, P. (1997). Sediment Distribution in the Nearshore Zone: GrainSize Evolution in Response to Shoreface Nourishment(Island of Terschelling, The Netherlands). *Estuarine, Coastal and Shelf Science*, *45*, 639–652.

Hallin, C., Almström, B., Larson, M., & Hanson, H. (2019). Longshore Transport Variability of Beach Face Grain Size: Implications for Dune Evolution. *Journal of Coastal Research*, *35*(4), 751–764.

Hanson, H. (2013). *Profilmätningar vid Löderups Strandbad och Ystad Strandskogen.* Teknisk Vattenresurslära, Lunds Universitet. (In Swedish).

Hanson, H., & Larson, M. (2008). Implications of extreme waves and water levels in the southern Baltic Sea. *Journal of Hydraulic Research*, *46*(2), 292–302.

Hassan, W. (2003). *Transport of size-graded and uniform sediment under oscillatory sheet-flow conditions.* Ph.D. Thesis, University of Twente.

Himmelstoss, E., Henderson, R., Kratzmann, M., & Farris, A. (2018). *Digital Shoreline Analysis System (DSAS) Version 5.0 User Guide.* U.S Geological Survey.

Kabuth, A., & Kroon, A. (2013). Wave energy fluxes and multidecadal shoreline changes in two coastal embayments in Denmark. *Coastal Dynamics 2013:* 7^{th} *International Conference on Coastal Dynamics*, 905–916.

Komar, P. (1998). *Beach processes and sedimentation* (Second edition). Prentice-Hall. Upper Saddle River, New Jersey, USA.

Kraus, N., Larson, M., & Wise, R. (1998). Depth of Closure in Beach-fill Design. *Coastal Engineering Technical Note CETN II-40*, *98*(3).

Lundbye, A. (2018). Kystsikring vækker begejstring: Faxe Ladeplads får ny 20 meter bred sandstrand. https://www.tv2east.dk/faxe/kystsikring-vaekker-begejstring-faxe-ladeplads-far-ny-20-meter-bred-sandstrand. *TV2 Øst*. 20 October. (In Danish).

Mangor, K., Fuchs, J., & Rand, P. (2010). *Fakse Ladeplads Lystbådehavn. Vurdering af virkningen af udvindelse af Fakse Ladeplads Lystbådehavn.* DHI. (In Danish).

Mase, H. (2001). Multi-directional Random Wave Transformation Model Based on Energy Balance Equation. *Coastal Engineering Journal*, *43*(4), 317–337.

Nam, P., Larson, M., Hanson, H., & Hoan, X. (2009). A numerical model of nearshore waves, currents, and sediment transport. *Coastal Engineering*, *56*, 1084–1096.

Narra, P., Coelho, C., & Fonseca, J. (2015). Sediment grain size variation along a cross-shore profile – representative d_{50}. *Journal of Coastal Conservation*, *19*(3), 307–320.

Nielsen, P. (2018). *Integreret uddybning og strandfodring ved Fakse Ladeplads*. (In Danish). University of Queensland.

Ramboll. (n.d.). Faxe Ladeplads – etablering af strand og kystbeskyttelse mod erosion. https://dk.ramboll.com/projects/rdk/faxe-ladeplads. Accessed: 2020-02-28.

Ramboll. (2016a). *Faxe Ladeplads - Modelrapport*. Ramboll, Copenhagen. (In Danish).

Ramboll. (2016b). *Faxe Ladeplads: Indledende vurderinger - hydraulik og badestrand*. Ramboll, Copenhagen. (In Danish).

Ramboll. (2017). *Faxe Ladeplads - Projektforslag*. Ramboll, Copenhagen. (In Danish).

Rosati, J. (2005). Concepts in Sediment Budgets. *Journal of Coastal Research*, *21*(2), 307–322.

Sørensen, T., Fredsøe, J., & Roed-Jakobsen, P. (1996). History of coastal engineering in Denmark. In Kraus, N.C (ed.) *History and Heritage of Coastal Engineering*, 103–141.

Stive, M., Aarninkof, S., Hamm, L., Hanson, H., Larson, M., Wijnberg, K., ... Capbianco, M. (2002). Variability of shore and shoreline evolution. *Coastal Engineering*, *47*, 211–235.

The Danish Environmental Protection Agency. (2017). *Faxe Kalk sejlrende, KLAP-TILLADELSE*. The Danish Environmental Protection Agency. Copenhagen. (In Danish).

U.S. Army Crops of Engineers. (1984). *Shore protection manual*. Coastal Engineering Research Center.

van Rijn, L. C. (2011). Coastal erosion and control. *Ocean & Coastal Management*, *54*, 867–887.

Wang, S. (2019). *Modelling Water Exchange in the Flommen Lagoon, South Sweden*. Division of Water Resources Engineering. Lund University.

A Appendix

A.1 Field Measurements: Coordinates for Measured Profile Lines

Start and end coordinates for profile lines P1-35 (located in the nourished area). Coordinate reference system: ETRS 1989 UTM Zone 32N.

Profile ID	**X_start**	**Y_start**	X_end	Y_end
P1	700882.0	6123053.1	700904.2	6123042.6
P2	700869.3	6123039.6	700892.5	6123023.4
P3	700865.3	6123023.6	700883.4	6123013.3
P4	700851.4	6123008.0	700873.3	6122996.3
P5	700852.3	6123001.5	700872.5	6122990.7
P6	700840.0	6122990.1	700862.8	6122976.9
P7	700838.7	6122981.3	700860.0	6122968.8
P8	700829.6	6122972.7	700851.2	6122956.0
P9	700820.7	6122958.8	700839.9	6122945.7
P10	700816.8	6122947.9	700836.2	6122932.3
P11	700805.3	6122931.2	700824.6	6122915.4
P12	700791.0	6122914.3	700813.6	6122898.4
P13	700780.1	6122898.8	700801.6	6122881.2
P14	700761.6	6122871.7	700785.0	6122856.3
P15	700754.3	6122857.8	700774.8	6122840.7
P16	700746.3	6122846.1	700768.2	6122831.2
P17	700728.5	6122824.6	700751.1	6122806.7
P18	700718.5	6122806.7	700748.2	6122784.5
P19	700706.4	6122793.9	700738.4	6122768.0
P20	700696.4	6122775.1	700726.4	6122751.1
P21	700690.9	6122766.6	700720.7	6122742.7
P22	700677.1	6122752.3	700709.9	6122725.9
P23	700662.4	6122736.5	700698.6	6122709.0
P24	700648.6	6122720.3	700687.4	6122692.6
P25	700635.4	6122703.8	700665.4	6122682.1
P26	700620.4	6122686.0	700655.4	6122665.0
P27	700609.2	6122672.3	700645.2	6122648.3
P28	700598.2	6122656.7	700634.4	6122632.0
P29	700591.4	6122649.0	700629.2	6122624.5
P30	700582.4	6122634.8	700615.2	6122606.1
P31	700572.9	6122620.0	700598.0	6122596.4
P32	700562.1	6122602.1	700587.9	6122578.8
P33	700552.5	6122581.0	700576.6	6122562.4
P34	700544.1	6122562.6	700564.4	6122546.6
P35	700528.5	6122543.2	700544.1	6122525.8

Start and end coordinates for profile lines PS1-6 (located in the area south of the outlet of Faxe Creek). Coordinate reference system: ETRS 1989 UTM Zone 32N.

Profile ID	X_start	Y_start	X_end	Y_end
PS1	700494.6	6122529.5	700518.4	6122511.7
PS2	700472.1	6122494.1	700527.4	6122463.9
PS3	700452.8	6122446.0	700498.5	6122419.6
PS4	700429.0	6122411.2	700480.1	6122388.5
PS5	700381.3	6122318.3	700410.2	6122305.2
PS6	700342.8	6122227.7	700371.9	6122217.1

A.2 Grain Size Distribution Curves

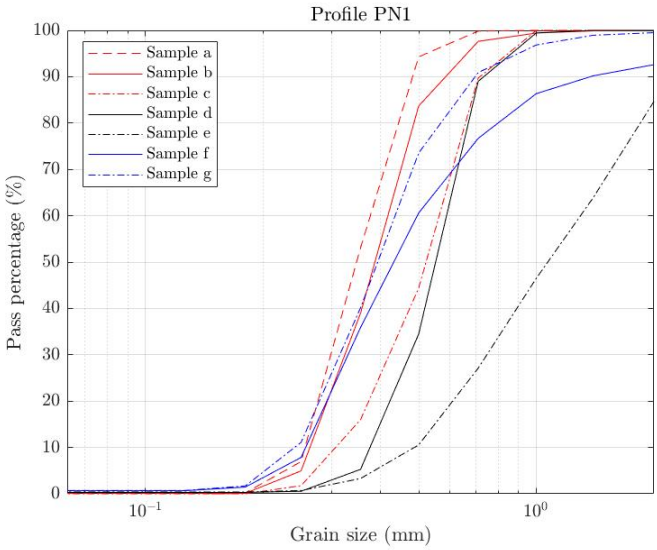

Figure A.1: Profile PN1, UTM-coordinates 701801.296; 6123385.078

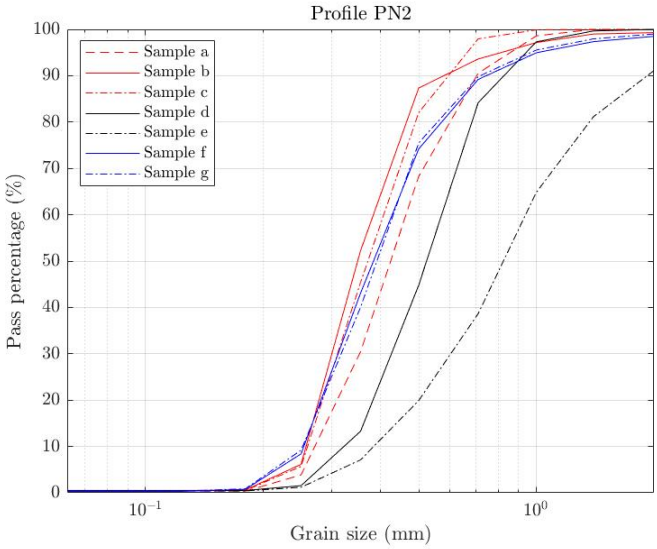

Figure A.2: Profile PN2, UTM-coordinates 701758.172; 6123338.801

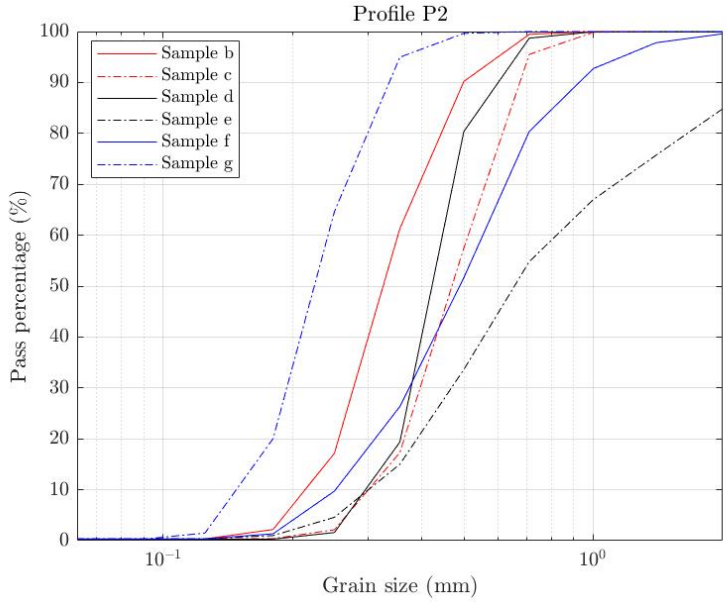

Figure A.3: Profile P2, UTM-coordinates 700871.605; 6123038.564

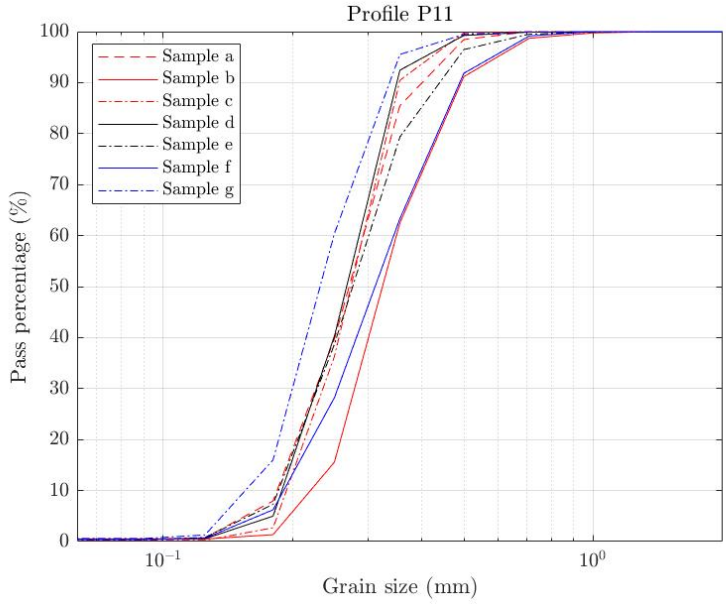

Figure A.4: Profile P11, UTM-coordinates 700805.605; 6122931.341

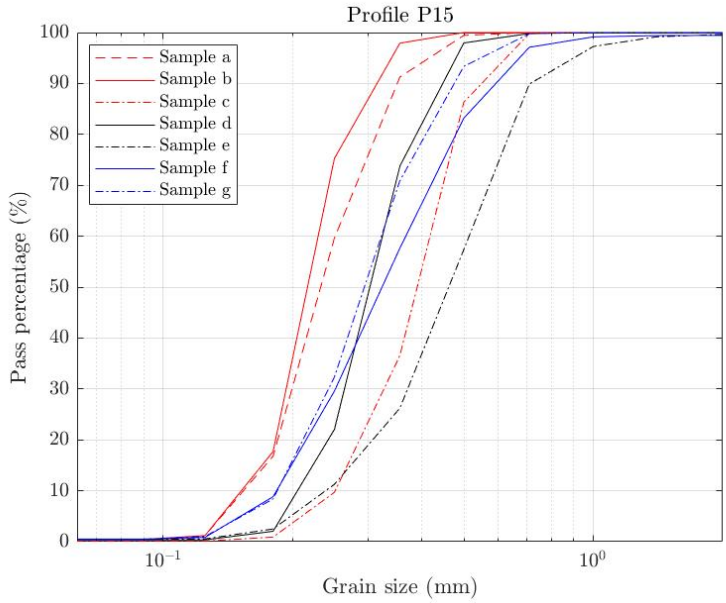

Figure A.5: Profile P15, UTM-coordinates 700753.753; 6122857.799

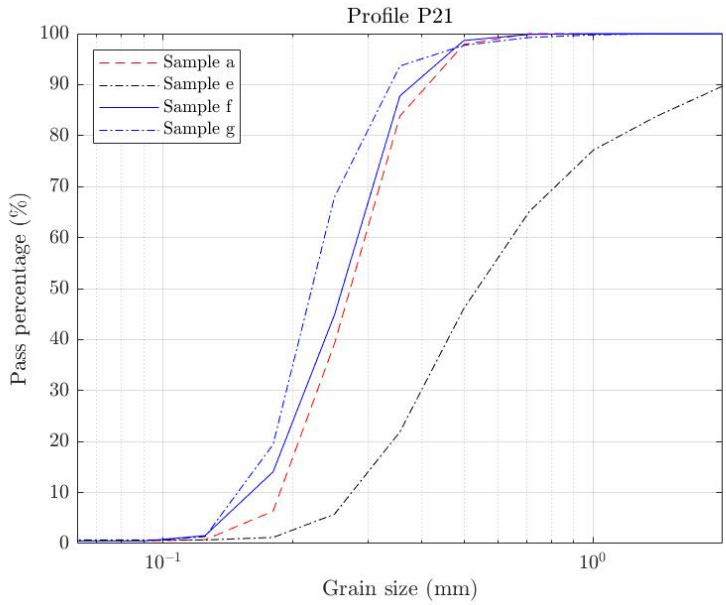

Figure A.6: Profile P21, UTM-coordinates 700689.999; 6122766.95

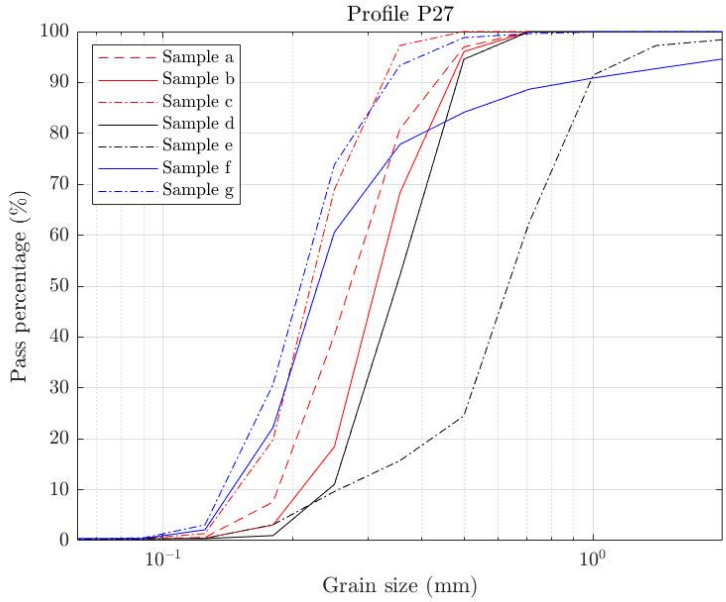

Figure A.7: Profile P27, UTM-coordinates 700609.879; 6122672.349

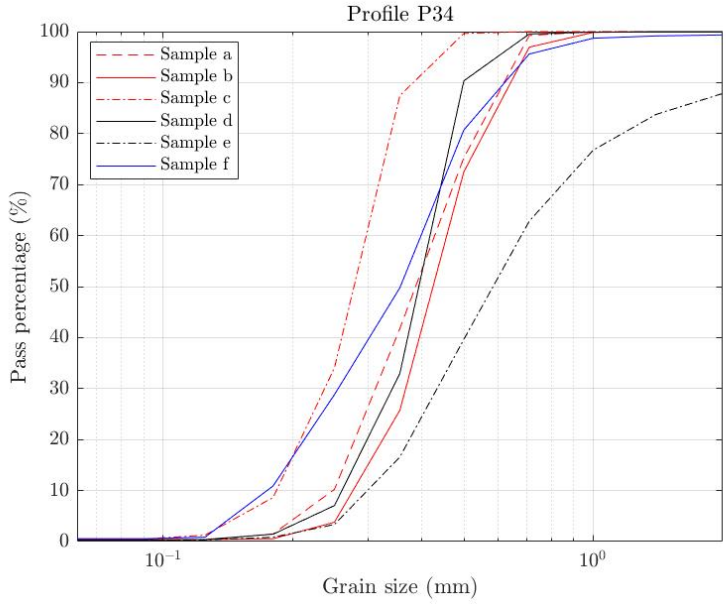

Figure A.8: Profile P34, UTM-coordinates 700544.102; 6122564.692

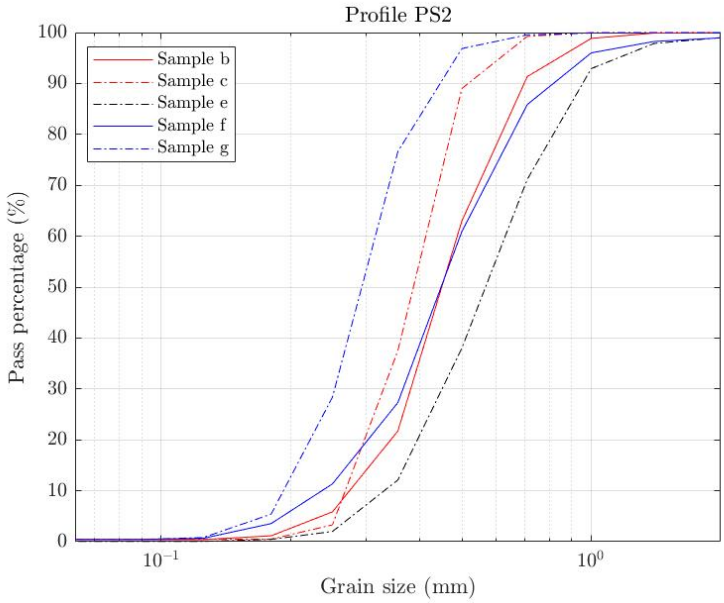

Figure A.9: Profile PS2, UTM-coordinates 700472.12; 6122494.103

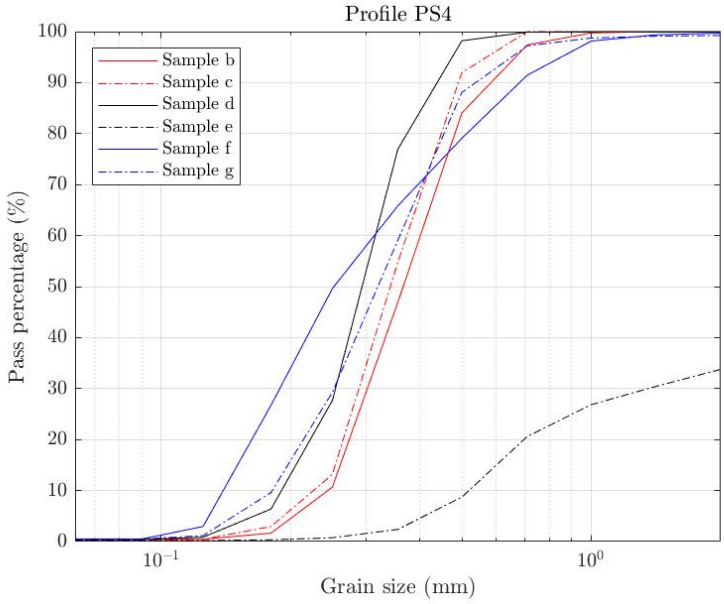

Figure A.10: Profile PS4, UTM-coordinates 700429.042; 6122411.226

A.3 Wave Climate 2012-2020

Left plots: Significant wave height (m) and water level (cm).

Right plots: Wave roses showing wave conditions.

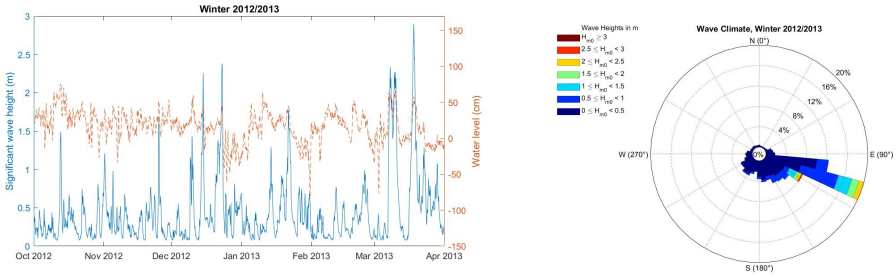

Figure A.11: October 2012 - March 2013.

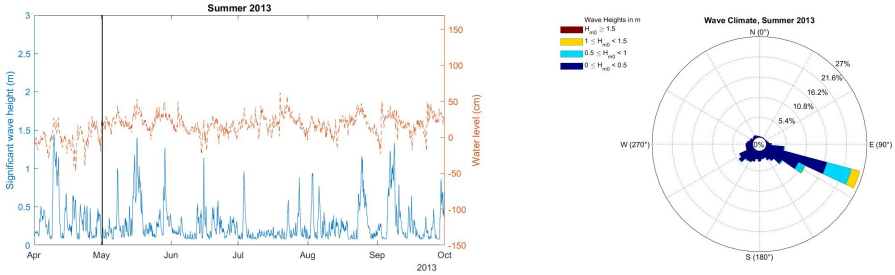

Figure A.12: April - September 2013. Black vertical line marks event of generated orthophoto (2 May 2013).

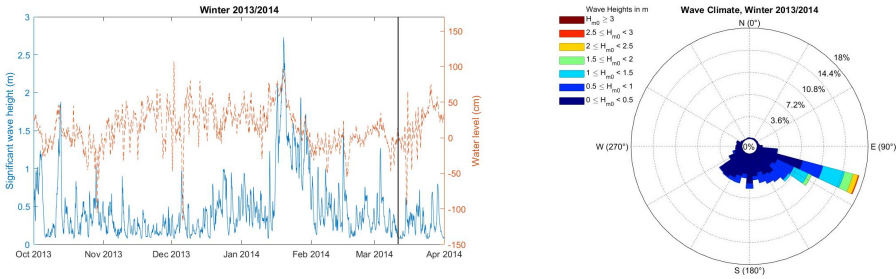

Figure A.13: October 2013 - March 2014. Black vertical line marks event of generated orthophoto (11 March 2014).

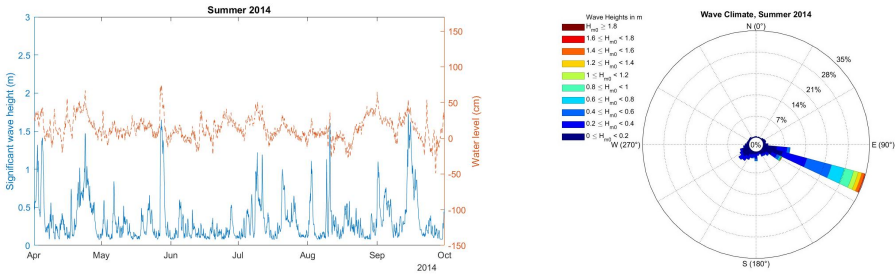

Figure A.14: April - September 2014.

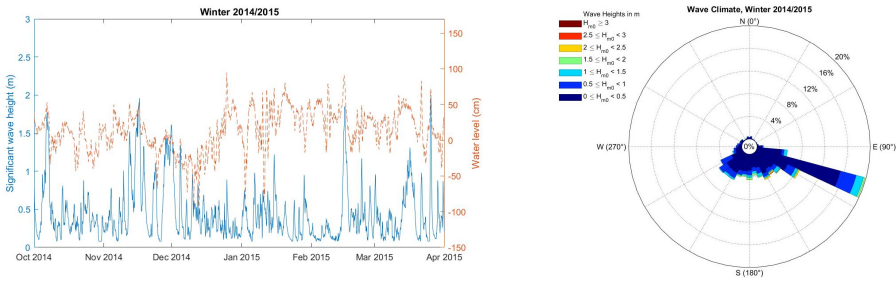

Figure A.15: October 2014 - March 2015.

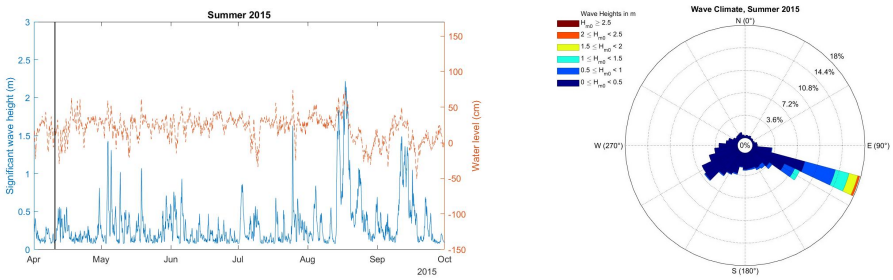

Figure A.16: April - September 2015. Black vertical line marks event of generated orthophoto (10 April 2015).

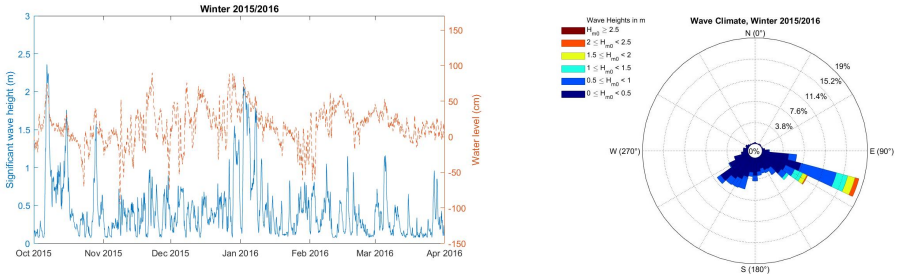

Figure A.17: October 2015 - March 2016.

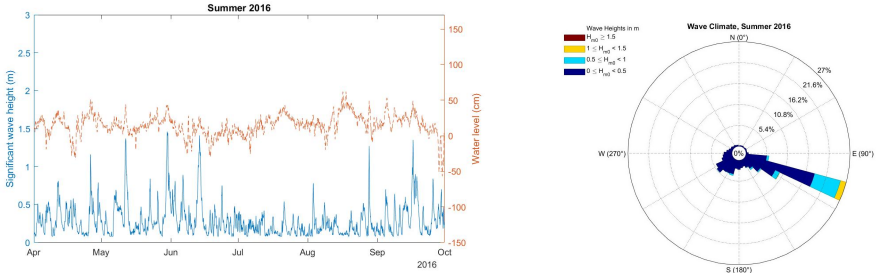

Figure A.18: April - September 2016.

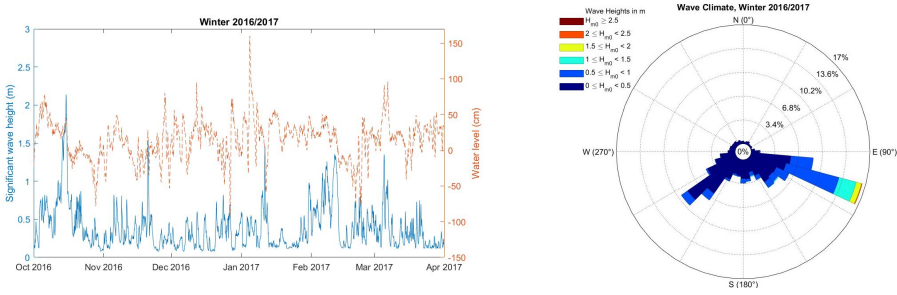

Figure A.19: October 2016 - March 2017

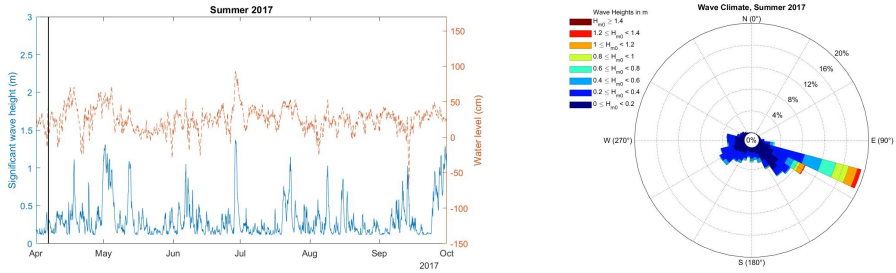

Figure A.20: April - September 2017. Black vertical line marks event of generated ortophoto (6 April 2017).

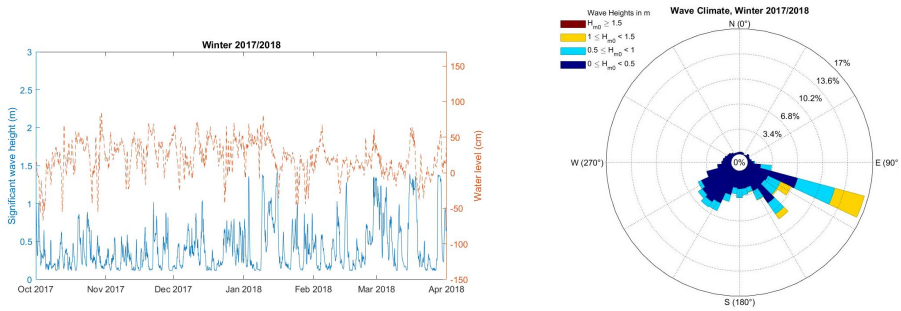

Figure A.21: October 2017 - March 2018.

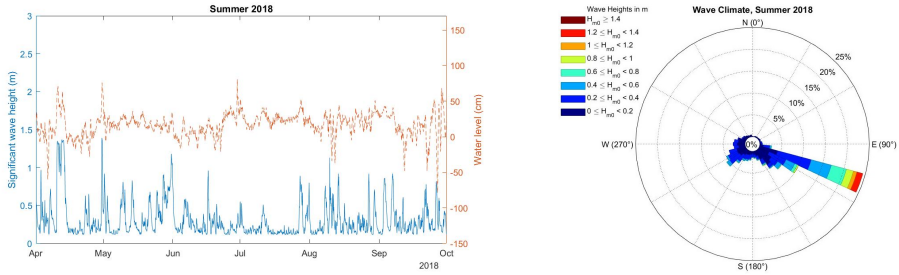

Figure A.22: April - September 2018.

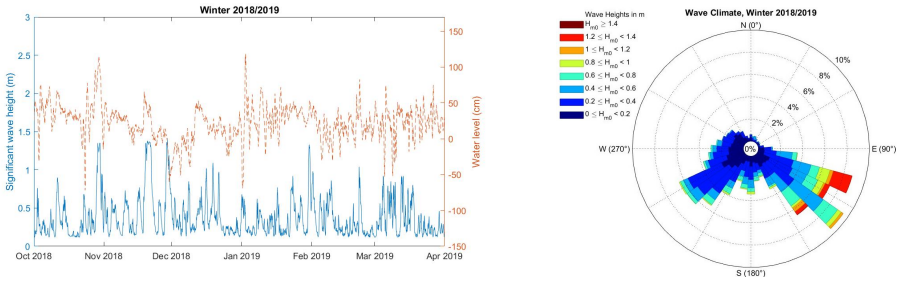

Figure A.23: October 2018 - March 2019.

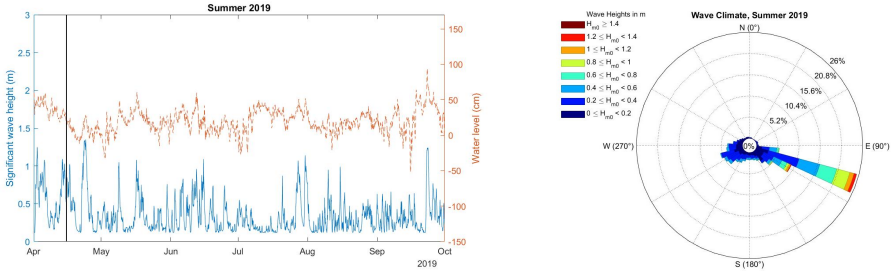

Figure A.24: April-September 2019. Black vertical line marks event of generated ortophoto (15 April 2019).

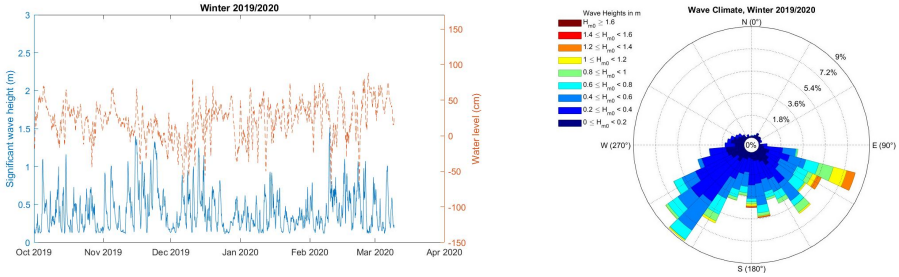

Figure A.25: October 2019 - March 2020.

A.4 Wave Transformation Model EBED

EBED is a nearshore wave transformation model produced by Mase (2001). The model is a multi-directional random wave transformation model, based on the energy balance equation and includes energy dissipation and diffraction terms. The energy equation at steady state, as formulated according to Mase (2001) is:

$$\frac{\partial\left(v_x S\right)}{\partial x}+\frac{\partial\left(v_y S\right)}{\partial y}+\frac{\partial\left(v_\theta S\right)}{\partial \theta}=\frac{\kappa}{2\omega}\left\{\left(CC_g\cos^2\theta S_y\right)_y-\frac{1}{2}CC_g\cos^2\theta S_{yy}\right\}-\varepsilon_b S$$

where S is the spectrum frequency, (x, y) are the longshore and cross-shore coordinates, θ is the angle measured anticlockwise from the $x-$axis, ω is the frequency, C is the phase speed, C_g is the group velocity and $v_{x,y,\theta}$ are the propagating velocities in the directions x, y and θ. The left side of the equation relates to the energy dissipation due to wave breaking, and ϵ_b is a dissipation coefficient. The parameter κ is a free parameter to control the effect of diffraction, hence the first term on the right side of the equation is introduced to represent the impact of diffraction.

The initial EBED model has shown to overestimate the computed wave parameters in the surf zone, compared to measurements. Nam, Larson, Hanson, and Hoan (2009) later modified the model by adopting a different approach to calculate the energy dissipation, to enhance the performance of the model. The modified energy balance equation at steady state, as formulated by Nam et al. (2009) is:

$$\begin{aligned}\frac{\partial\left(v_x S\right)}{\partial x}+\frac{\partial\left(v_y S\right)}{\partial y}+\frac{\partial\left(v_\theta S\right)}{\partial \theta}=&\frac{\kappa}{2\omega}\left\{\left(CC_g\cos^2\theta S_y\right)_y-\frac{1}{2}CC_g\cos^2\theta S_{yy}\right\}\\&-\frac{K}{h}C_g\left(S-S_{\text{stab}}\right)\end{aligned}$$

where h is the still water level, K is the dimensionless decay coefficient, S_{stab} is the stable wave spectrum density which is dependent on the stable wave height, H_{stab}. H_{stab} is equal to Γh and Γ is a dimensionless empirical coefficient. By assuming that the spectrum density S and the stable spectrum density S_{stab} are functions of H_s^2 and H_{stab}, the dissipation term, i.e. the final term in the equation by Nam et al. (2009), can be re-written as:

$$D_{\text{diss}}=\frac{K}{h}C_g S\left[1-\left(\frac{\Gamma h}{H_{\text{s}}}\right)^2\right]$$

Values of the decay coefficient K and the empirical coefficient Γ has been determined based on observations (Nam et al., 2009), and are recommended to be:

$$\begin{array}{ll} \Gamma = 0.45, \quad K = \frac{3}{8}(0.3 - 19.2s) & s < 0 \\ \Gamma = 0.45 + 1.5s, \quad K = \frac{3}{8}(0.3 - 0.5s) & s \geq 0 \end{array}$$

where s is the bottom slope.

The nearshore wave transformation model computes three wave parameters in each cell of the grid; significant wave height H_s, significant wave period T_s and mean wave direction $\bar{\theta}$.